RESOURCE GEOLOGY

doi: 10.1111/rge.12003 *Resource Geology* Vol. 63, No. 2: 166–187

Original Article

First Reliable Re–Os Ages of Pyrite and Stable Isotope Compositions of Fe(-Cu) Deposits in the Hami Region, Eastern Tianshan Orogenic Belt, NW China

Xiao-Wen Huang,[1,2] Liang Qi,[1] Jian-Feng Gao[3] and Mei-Fu Zhou[3]

[1]*State Key Lab of Ore Deposit Geochemistry, Institute of Geochemistry, Chinese Academy of Sciences, Guiyang, China and* [2]*Graduate University of the Chinese Academy of Sciences, Beijing, China and* [3]*Department of Earth Sciences, The University of Hong Kong, Hong Kong SAR, China*

Abstract

The Eastern Tianshan Orogenic Belt (ETOB) in NW China is composed of the Dananhu–Tousuquan arc belt, the Kanggurtag belt, the Aqishan–Yamansu belt and the Central Tianshan belt from north to south. These tectonic belts have formed through arc–continent or arc–arc collisions during the Paleozoic. A number of Fe(-Cu) deposits in the Aqishan–Yamansu belt, including the Heifengshan, Shuangfengshan and Shaquanzi Fe(-Cu) deposits, are associated with Carboniferous–Early Permian volcanic rocks and are composed of vein-type magnetite ores. Metallic minerals are dominated by magnetite and pyrite, with minor chalcopyrite. Calcite, chlorite, and epidote are the dominant gangue minerals. Pyrite separates of ores from those three deposits have relatively high and variable Re contents ranging from 3.7 to 184 ppb. All pyrite separates have very low common Os, allowing us calculation of single mineral model ages for each sample. Pyrite separates from the Heifengshan Fe deposit have an ^{187}Re–^{187}Os isochron age of 310 ± 23 Ma (MSWD = 0.04) and a weighted mean model age of 302 ± 5 Ma (MSWD = 0.17). Those from the Shuangfengshan Fe deposit have an isochron age of 295 ± 7 Ma (MSWD = 0.28) and a weighted mean model age of 292 ± 5 Ma (MSWD = 0.33). The Shaquanzi Fe-Cu deposit has pyrite with an isochron age of 295 ± 7 Ma (MSWD = 0.26) and a weighted mean model age of 295 ± 6 Ma (MSWD = 0.23). Pyrite separates from these Fe(-Cu) deposits have $\delta^{34}S_{CDT}$ ranging from –0.41‰ to 4.7‰ except for two outliers. Calcite from the Heifengshan Fe deposit and Shaquanzi Fe-Cu deposit have similar C and O isotope compositions with $\delta^{13}C_{PDB}$ and $\delta^{18}O_{SMOW}$ ranging from –5.5‰ to –1.0‰ and from 10‰ to 12.7‰, respectively. These stable isotopic data suggest that S, C, and O are magmatic-hydrothermal in origin. The association of low-Ti magnetite and Fe/Cu-sulfides resembles those of Iron–Oxide–Copper–Gold (IOCG) deposits elsewhere. Our reliable Re–Os ages of pyrite suggest that the Fe(-Cu) deposits in the Aqishan–Yamansu belt formed at ~296 Ma, probably in a back-arc extensional environment.

Keywords: Eastern Tianshan, Fe(-Cu) deposits, NW China, Pyrite, Re–Os dating, Stable isotopes.

Received 25 February 2012. Accepted for publication 3 July 2012.

Corresponding author: L. Qi, State Key Lab of Ore Deposit Geochemistry, Institute of Geochemistry, Chinese Academy of Sciences, 46th Guanshui Road, Guiyang 550002, China. Email: qilianghku@hotmail.com

1. Introduction

The Paleozoic Tianshan Orogenic Belt (TOB) has been an important target for mineral exploration in China (Wang *et al*., 2006a). Numerous Fe(-Cu) deposits including the Yamansu, Heifengshan, Shuangfengshan, and Shaquanzi Fe(-Cu) deposits in the Hami region constitute the Aqishan–Yamansu metallogenic belt (Gao *et al*., 1993; Che *et al*., 1994; Hua, 2001; Hua *et al*., 2002; Qin *et al*., 2002; Wang *et al*., 2006a). These Fe(-Cu) deposits have been described mainly in Chinese literature (Song *et al*., 1983; He *et al*., 1994a; Jiang *et al*., 2002; Xiao, 2003; Fang *et al*., 2006a, b). However, their origin and tectonic settings are poorly understood.

In particular, determining the age of hydrothermal deposits is difficult because there are no suitable hydrothermal minerals for isotopic dating. It has been documented that the Re–Os isotopic system is robust for dating hydrothermal activities (Walker *et al*., 1994; Suzuki *et al*., 1996; Stein *et al*., 1998, 2000; Mathur *et al*., 1999; Brenan *et al*., 2000). Molybdenite is particularly suitable for Re–Os isotopic dating, however, many hydrothermal deposits do not contain molybdenite. As an alternative, pyrite commonly occurs in many hydrothermal deposits and has been recently used for Re–Os dating of different types of hydrothermal deposits (Stein *et al*., 1998, 2000; Mathur *et al*., 1999; Morgan *et al*., 2000; Arne *et al*., 2001; Barra *et al*., 2002; Zhang *et al*., 2005; Cardon *et al*., 2008; Selby *et al*., 2009; Nozaki *et al*., 2010).

In this paper, we report the well-fitted Re–Os isochron ages of pyrite from the Heifengshan, Shuangfengshan and Shaquanzi Fe(-Cu) deposits of the Aqishan–Yamansu belt, NW China. The new dataset indicates that these deposits formed at ~296 Ma and demonstrates that the Re–Os chronometer of pyrite can be a reliable tool to date hydrothermal deposits. Combined with the sulfur isotope of pyrite, and the carbon and oxygen isotopes of calcite, the ages of these deposits are used to constrain the origin of the Fe(-Cu) deposits and metallogeny of the TOB.

2. Geologic background

2.1 Regional geology

The TOB extends west–east for about 1500 km in the Central Asian Orogenic Belt (Fig. 1a). The TOB formed by subduction, accretion and collision of various continental blocks between the northern Siberia and Tarim-North China cratons. The final amalgamation of these blocks occurred in the Late Carboniferous (Ma *et al*., 1993, 1997; Ji *et al*., 1994; Yang *et al*., 1997; Qin *et al*., 2002; Xia *et al*., 2008a) or Permian (Xiao *et al*., 2009).

The TOB comprises the North, Central, and South Tianshan belts, separated by major E–W-trending faults (Fig. 1b). The North Tianshan belt consists of Carboniferous calc-alkaline volcanic and sedimentary rocks, intruded by Permian–Carboniferous mafic and intermediate-felsic plutons. The Carboniferous rocks may have formed by northward or southward subduction of the oceanic crust (Pirajno *et al*., 2008). The Central Tianshan belt is a wedge-shaped zone with late Proterozoic basement, which may have been part of the microcontinents (Zhang *et al*., 1984). The South Tianshan belt contains fragments of oceanic crust materials in fault contacts with middle Silurian to middle Carboniferous sandstone, shale, chert and limestone, which were possibly deposited on a passive margin of the northern Tarim block (Carroll *et al*., 1995).

Several approximately E–W-trending faults separate the eastern part of the TOB into four main tectonic units from north to south, the Dananhu–Tousuquan arc belt, the Kanggurtag belt, the Aqishan–Yamansu belt and the Central Tianshan belt (He *et al*., 1994b; Gao *et al*., 1998; Qin *et al*., 2002, 2003a; Xiao *et al*., 2004; Wang *et al*., 2006a, b; Qi *et al*., 2008) (Fig. 1c).

The Dananhu–Tousuquan arc belt is made up of the Devonian to Carboniferous island arc volcanic rocks. The Devonian strata are composed of basaltic to andesitic volcanic rocks, with local carbonate and calcareous mudstone. Overlying these rocks is the late Carboniferous Tuwu Formation of greywacke and tuff intercalated with carbonates. The Tuwu Formation is overlain by Permian basalt, tuff and volcanic breccia, and Jurassic terrestrial clastic rocks (Mao *et al*., 2005).

In the Kanggurtag belt, there are mylonite, tectonic lenses, and breccias formed along early extensional faults (Qin *et al*., 2002; Xu *et al*., 2003). The Carboniferous strata of the Kanggurtag belt are composed of fine-grained sandstone and carbonaceous argillite. Numerous mafic and ultramafic intrusions include the Permian Huangshan, Xiangshan, and Hulu intrusions (Qin *et al*., 2003b; Han *et al*., 2004; Zhou *et al*., 2004). The Kanggurtag belt contains ophiolitic fragments and was thought to mark a suture zone separating the Siberia craton to the north from the Tarim block to the south (Ji *et al*., 1994; Yang *et al*., 1996; Ma *et al*., 1997; Zhou *et al*., 2001). The Kanggurtag belt was also thought to be an inter-arc basin between the Dananhu–Tousuquan and Yamansu arcs (Ma *et al*., 1997; Shu *et al*., 2002).

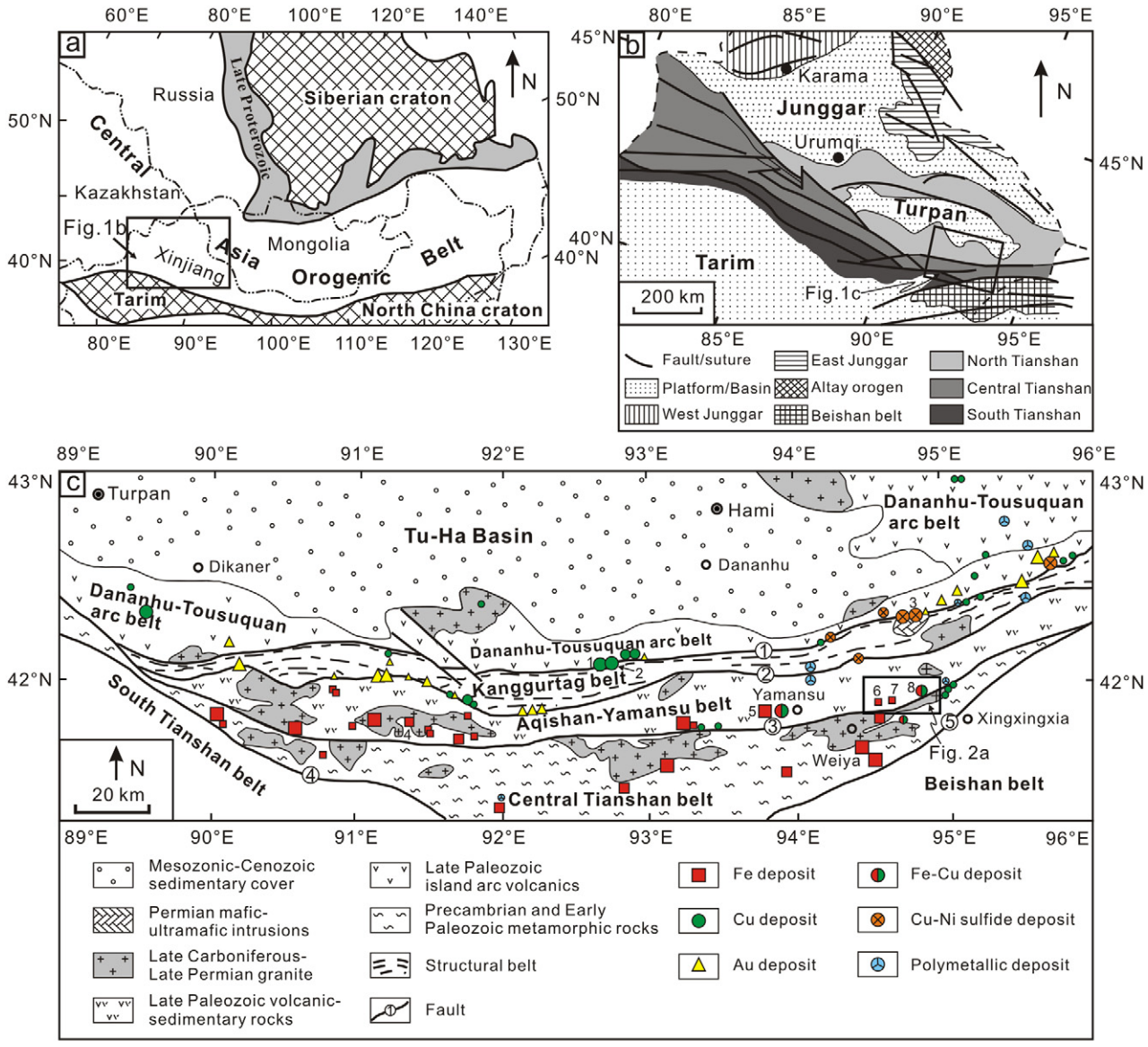

Fig. 1 (a) Location of the study area in the Central Asia Orogenic Belt (modified from Zhang *et al.*, 2009). (b) A map showing geologic units of the Tianshan Orogenic Belt (modified from Pirajno *et al.*, 2008). (c) A simplified geological map of the Eastern Tianshan Orogenic Belt (after Yang *et al.*, 1996; Mao *et al.*, 2005). Faults (Number in circle): 1-Kanggurtag-Huangshan fault; 2-Kushui fault; 3-Shaquanzi fault; 4-Toksun-Gangou fault; 5-Xingxingxia fault. Mineral deposits: 1-Tuwu porphyry Cu deposit; 2-Yandong porphyry Cu deposit; 3-Huangshan Cu-Ni sulfide deposit; 4-Bailingshan skarn Fe-Cu deposit; 5-Yamansu Fe deposit; 6-Heifengshan Fe deposit; 7-Shuangfengshan Fe deposit; 8-Shaquanzi Fe-Cu deposit.

The Aqishan–Yamansu belt is bounded to the north by the Kushui fault from the Kanggurtag belt and to the south by the Shaquanzi fault. The Aqishan–Yamansu belt comprises a 5 km thick succession of the Lower Carboniferous Yamansu Formation of bimodal volcanic rocks, the middle Carboniferous Shaquanzi Formation of clastic rocks and andesitic tuff, and the upper Carboniferous Tugutublak Formation of intercalated carbonate. Permian marine and terrestrial clastic rocks are intercalated with bimodal volcanic rocks and carbonates (Mao *et al.*, 2005). Because of large volumes of intra-plate rift-related volcanic rocks in the

Aqishan–Yamansu belt, this belt has been thought to be an early Carboniferous rift zone (Xiao *et al*., 1992; Qin *et al*., 2002; Xia *et al*., 2003, 2008b). However, it is also thought to be an island arc belt (Yan, 1985; Yang *et al*., 1996, 1999; Ma *et al*., 1997).

The Central Tianshan belt in Eastern Tianshan has been regarded as a composite volcanic arc, which is composed of Precambrian basement rocks of amphibolite facies, overlain by calc-alkaline basaltic andesite, volcanoclastics, minor I-type granite, and granodiorite (Xiao *et al*., 2004). The Precambrian basement consists of gneiss, quartz schist, migmatite, and marble.

Carboniferous–Permian mafic–felsic intrusions and Carboniferous volcanic rocks (c. 354–306 Ma) are widespread in the TOB (Xia *et al*., 2002a, b, 2003, 2004). Late Paleozoic granites and mafic intrusions were emplaced at c. 270–300 Ma (Zhou *et al*., 2004, 2010).

2.2 Ore deposits of the ETOB

The Eastern Tianshan Orogenic Belt (ETOB) hosts numerous mineral deposits including porphyry Cu deposits in the Dananhu–Tousuquan arc belt, gold deposits and Cu-Ni sulfide deposits in the Kanggurtag belt, and Fe–Cu–Ag polymetallic deposits in the Aqishan–Yamansu belt and Central Tianshan belt (Fig. 1c). These mineral deposits are closely associated with igneous rocks in space and time (Ma *et al*., 1997; Yang *et al*., 1997; Qin *et al*., 2002; Wang *et al*., 2006b). The Tuwu and Yandong porphyry Cu deposits in the Dananhu–Tousuquan arc belt formed at 341–347 Ma (Qin *et al*., 2002; Rui *et al*., 2002). Gold deposits in the Kanggurtag belt have ages ranging from 276 to 300 Ma (Li *et al*., 1998; Zhang *et al*., 2004), whereas the Hulu, Huangshan, Tulaergen and Xiangshan Cu–Ni sulfide deposits in the belt are hosted in 270–300 Ma mafic intrusions (Qin *et al*., 2002; Mao *et al*., 2002b; Zhou *et al*., 2004; Chen *et al*., 2005; Han *et al*., 2010; San *et al*., 2010). The large size Yamansu Fe deposit is located in the west part of the Aqishan–Yamansu belt, whose wall rock andesitic porphyry has a whole-rock Rb–Sr isochron age of 374 ± 44 Ma, whereas garnet-epidote mineral separates have a Sm–Nd isochron age of 352 ± 46 Ma (Li & Chen, 2003). The Bailingshan skarn Fe(-Cu) deposit in the Aqishan–Yamansu belt has a Rb–Sr age of 286 ± 12 Ma for ore-bearing quartz veins (Li & Liu, 2003). The Weiquan Ag polymetallic skarn deposit in the Aqishan–Yamansu belt is genetically related to the adjacent Bailingshan granitoid pluton, which has a SHRIMP zircon U–Pb age of 297 ± 3 Ma (Wang *et al*., 2005).

3. Geology of the Fe(-Cu) deposits

There are numerous Fe(-Cu) deposits in the Aqishan–Yamansu belt. The large-size Bailingshan and Yamansu Fe(-Cu) deposits are considered to be skarn type deposits (Mao *et al*., 2005). The Heifengshan, Shuangfengshan, and Shaquanzi Fe(-Cu) deposits are all located along the regional Shaquanzi fault in a small district (Fig. 1c). These deposits share common geological features and mineralization styles. Although their genesis may be linked with magmatism, their ages of formation remain unknown, and it is critical to the understanding of their origin. Despite enormous metallogenic potential, other deposits are not known in the literature.

3.1 Heifengshan and Shuangfengshan Fe deposits

Both the Heifengshan and Shuangfengshan Fe deposits southeast of Hami city contain Fe-rich ores with an average ore grade of 44% Fe (Fig. 1c). The Heifengshan Fe deposit is hosted in the middle Carboniferous Shaquanzi Formation of basaltic to rhyolitic volcanic rocks and volcanoclastic rocks, interlayered with mudstone, sandstone, tuff, and tufaceous sandstone (Fig. 2a). The Shuangfengshan Fe deposit is hosted in the early Carboniferous bimodal volcanic and clastic rocks of the Yamansu Formation (Fig. 2a), mainly consisting of andesitic tuff, andesitic tuff breccia, limestone, potash-keratophyre, and felsic porphyry. These two deposits are composed of vein-type and lens-shaped ore hosted in the transitional zone between volcanic and sedimentary rocks. Ore bodies are locally intruded by dioritic dikes, leading to the formation of epidote skarn (Jiang *et al*., 2002).

The magnetite ores of the Heifengshan and Shuangfengshan deposits have ore minerals of magnetite and pyrite, and gangue minerals of calcite, chlorite, and epidote. The ores have a variety of textures, including massive, disseminated and banded textures. Massive ores from the Heifengshan Fe deposit comprise approximately 60–80 vol.% magnetite, 5–10 vol.% pyrite and 10–20 vol.% calcite and 5 vol.% chlorite (Fig. 3a). The pores of massive ores are usually filled by calcite and chlorite (Fig. 3b). Disseminated ores from the Heifengshan Fe deposit are composed of about 20–30 vol.% magnetite, 20–30 vol.% pyrite, 10–20 vol.% calcite and 10–20 vol.% chlorite (Fig. 3c). Pyrite occurs mostly within or along the grain boundary of calcite (Fig. 4a). Banded ores from the Heifengshan Fe deposit

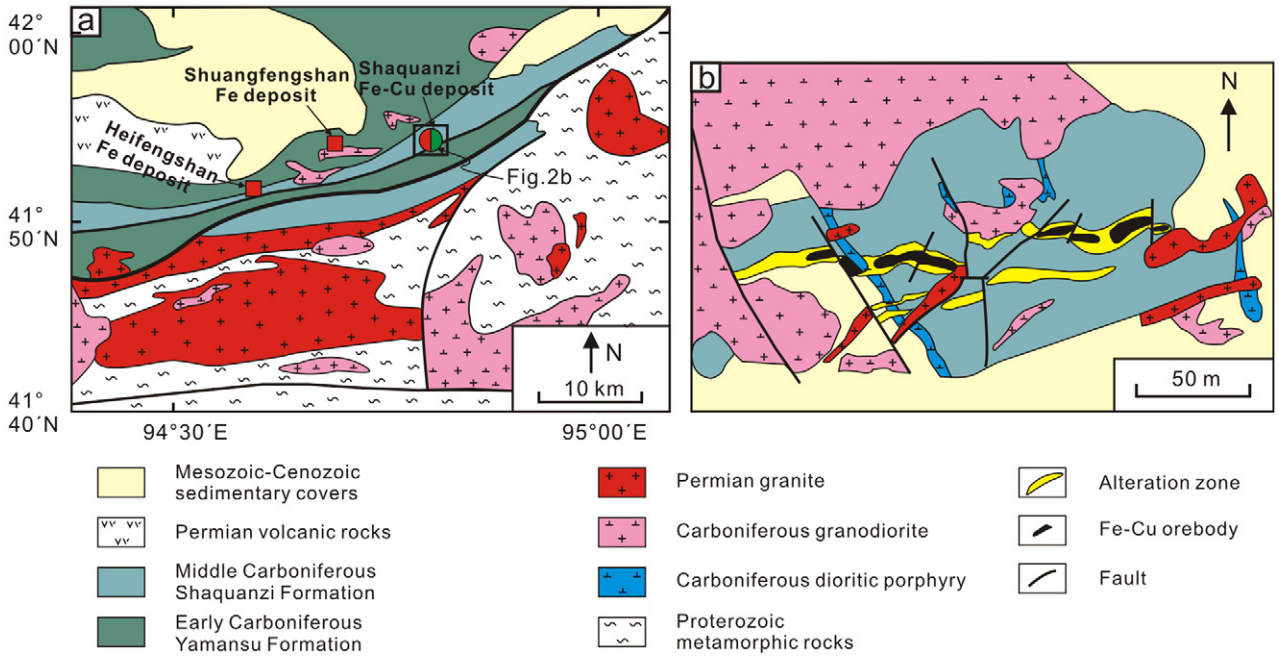

Fig. 2 (a) Locality map of the Yamansu-Shaquanzi metallogenic belt (modified from Chen, 2006). (b) Geological map of the Shaquanzi Fe-Cu deposit (after Xu *et al.*, 2010).

consist of 70–80 vol.% magnetite and minor chlorite (Fig. 3d). Minor malachite is also observed in the Heifengshan Fe deposit (Fig. 3e). Massive ores from the Shuangfengshan Fe deposit comprise magnetite, pyrite, and calcite (Fig. 3f). Massive ores are filled by calcite, forming the miarolitic structure (Fig. 3g). Massive ores are sometimes brecciated and cemented by calcite (Fig. 3h). Disseminated ores from the Shuangfengshan Fe deposit are composed of magnetite and pyrite (Fig. 3i, j). Vein-type pyrite is also observed in some ores, indicative of multiple hydrothermal activities (Fig. 4b).

3.2 Shaquanzi Fe-Cu deposit

The Shaquanzi Fe–Cu deposit consists of orebodies hosted in the middle Carboniferous Shaquanzi Formation (Fig. 2b). The Shaquanzi Fe–Cu deposit contains Fe–Cu ores with grades of 25–36% Fe and 0.5–2.3 wt.% Cu (Zeng, 1962; Fang *et al.*, 2006a). Orebodies are usually lens-shaped and controlled by faults. There are more than four orebodies which are 5 to 500 m in length and 2 to 6 m in thickness (a maximum thickness of 11.3 m). The copper-rich orebody occurs at a depth of 20 to 40 m, with a general length of 230 m and thickness of 2 to 5 m. It has a maximum depth of 165 m and a maximum thickness of 6.13 m. Extensive hydrothermal alteration include chloritization, epidotization, carbonation, pyritization, and albitization. Metallic minerals are magnetite, pyrite, and minor chalcopyrite, whereas gangue minerals include chlorite, epidote, calcite, and quartz. Massive ores are composed of magnetite, pyrite, chalcopyrite, and calcite (Fig. 3k). Granular pyrite is also randomly dispersed in massive ores (Fig. 3l). Copper-bearing minerals such as chalcopyrite often occur in the fracture of pyrite grains (Fig. 4c, d). Disseminated ores have a mineral assemblage of magnetite ± pyrite ± chalcopyrite ± chlorite ± calcite ± quartz (Fig. 4e, f).

4. Analytical method

4.1 Re–Os isotope analyses

Samples in this study were taken from open pit or drill cores of the Heifengshan, Shuangfengshan, and Shaquanzi deposits. Pyrite for Re–Os analyses is separated from massive and disseminated ores. Ores are carefully selected for pyrite separation. All pyrite separates were then hand-picked under binocular microscope. Pyrite separates for Re–Os analyses are free from weathering or oxidation. Vein-type pyrite was

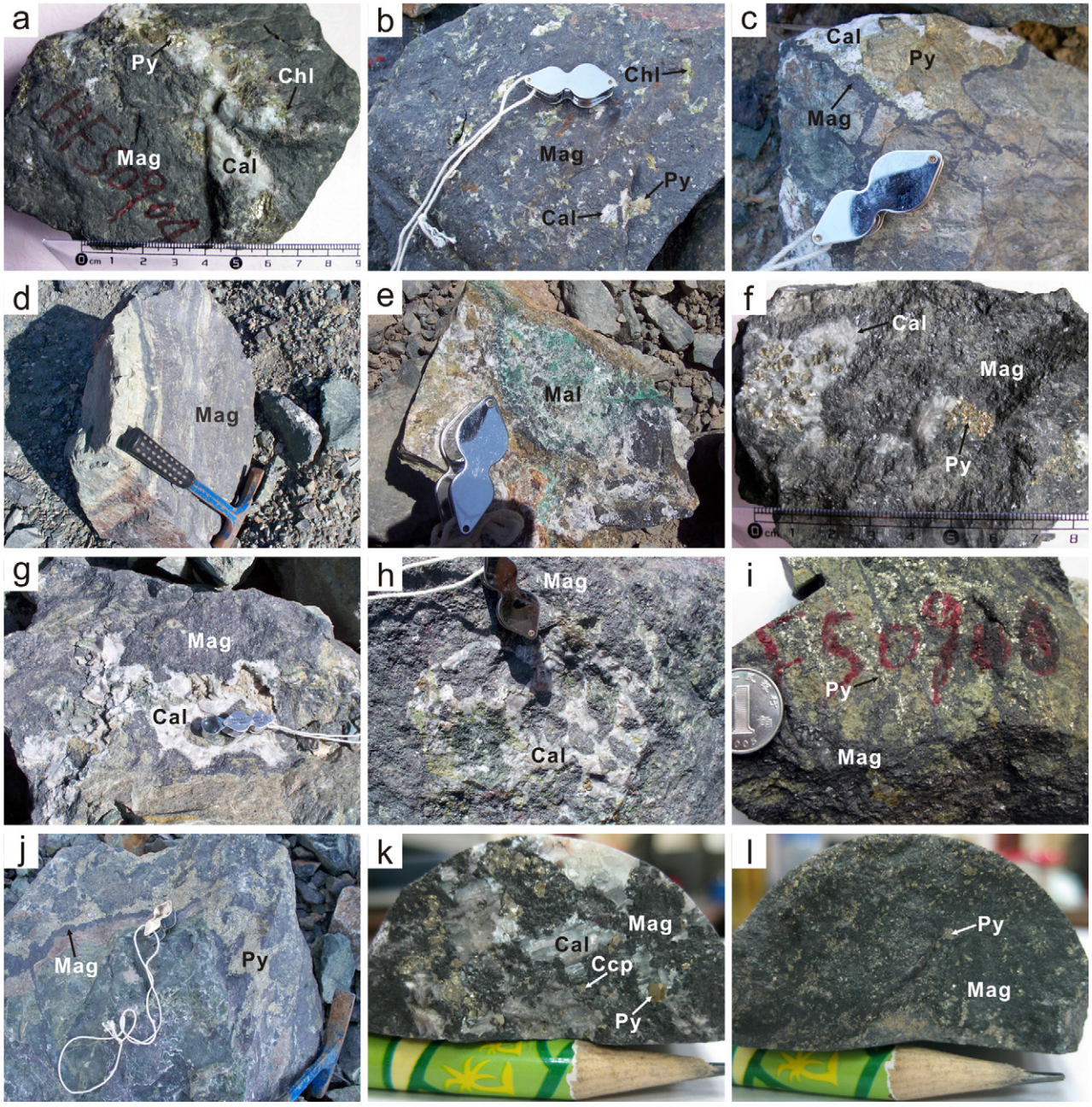

Fig. 3 Field photographs and hand specimen of ores. (a) Massive ores from the Heifengshan Fe deposit comprise magnetite, pyrite, calcite and chlorite. (b) The pore of massive ores from the Heifengshan Fe deposit are filled by calcite and chlorite. (c) Disseminated ore from the Heifengshan Fe deposit is composed of magnetite, pyrite, and calcite. (d) Banded ores from the Heifengshan Fe deposit. (e) Minor malachite in the Heifengshan Fe deposit. (f) Massive ore from the Shuangfengshan Fe deposit comprises magnetite, pyrite, and calcite. (g) Calcite-filled structure of massive ore from the Shuangfengshan Fe deposit. (h) Brecciated structure, massive ore from the Shuangfengshan Fe deposit is sometimes cemented by calcite. (i) Disseminated ore from the Shuangfengshan Fe deposit are composed of magnetite and pyrite. (j) Disseminated ore from the Shuangfengshan Fe deposit, the pyrite vein grows in directions nearly parallel to the magnetite vein. (k) Massive ore from the Shaquanzi Fe-Cu deposit is composed of magnetite, chalcopyrite, euhedral pyrite, and calcite. (l) Massive ore from the Shaquanzi Fe-Cu deposit contains disseminated pyrite. Abbreviations: Mag, magnetite; Py, pyrite; Ccp, chalcopyrite; Cal, calcite; Chl, chlorite; Mal, malachite.

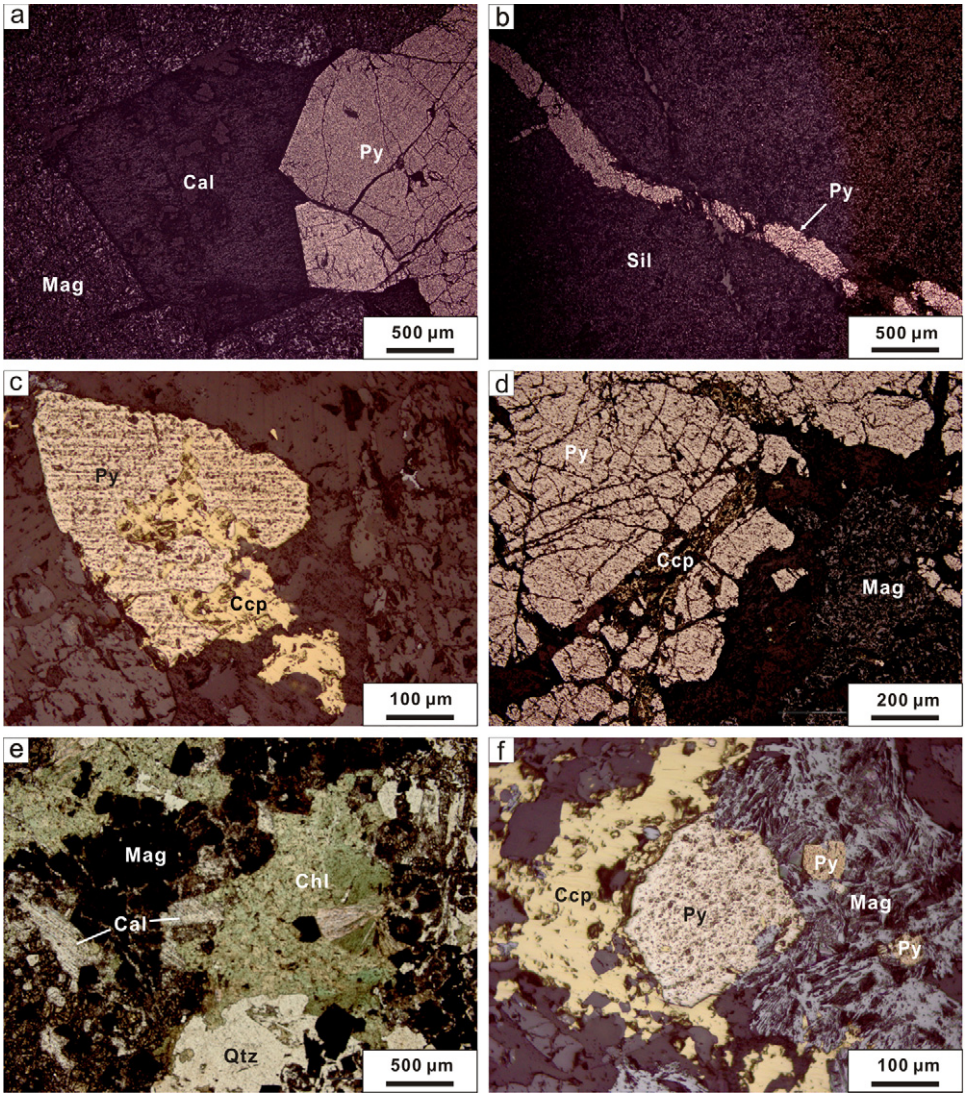

Fig. 4 Photomicrographs of ores. (a) Disseminated ore from the Heifengshan Fe deposit is composed of magnetite, pyrite and calcite (under polarized and reflected light). (b) Veinlet of pyrite crosscuts the silicate minerals of the Shuangfengshan ores (under reflected light). (c) Chalcopyrite replaced early pyrite (under reflected light). (d) Minor chalcopyrite infills preexisting fracture of pyrite grains in the Shaquanzi ores (under reflected light). (e) Disseminated ore from the Shaquanzi Fe-Cu deposit has a mineral assemblage of magnetite, chlorite, calcite, and quartz (under polarized light). (f) Ore from the Shaquanzi Fe–Cu deposit has a mineral assemblage of magnetite, pyrite and chalcopyrite (under reflected light). Abbreviations: Mag, magnetite; Py, pyrite; Ccp, chalcopyrite; Cal, calcite; Chl, chlorite; Sil, silicate; Qtz, quartz.

not chosen for Re–Os analyses because of uncertain genesis (Fig. 4b). Pyrite grains replaced by chalcopyrite (Fig. 4c) and minor chalcopyrite along preexisting fracture of pyrite grains (Fig. 4d) are observed in ores from the Shaquanzi Fe–Cu deposit. These pyrite grains were not chosen for Re–Os analyses because of impurity. Most of the pyrite grains range in size from 250 to 800 μm.

Re–Os isotopic analyses were performed in the State Key Lab of Ore Deposit Geochemistry, Institute of Geochemistry, Chinese Academy of Sciences. A detailed description of the Re–Os isotope analytical procedure is available in Qi *et al*. (2010). Briefly, approximately 0.5 g of pyrite separates were accurately weighed and placed in a 120 mL Carius tube. The Carius tube was immersed in an ice-water bath when

Table 1 Blank level (ng), detection limits (DL, ppb) and analytical results for molybdenite reference materials, HLP and JDC

	Blank (ng)	DL (3σ, ppb)	JDC (Average ± SD, n = 5)	Certified†	HLP (Average ± SD, n = 5)	Certified†
Re (ppm)	0.0064	0.0010	17.22 ± 0.19	17.39 ± 0.32	283.1 ± 3.2	238.8 ± 6.2
Os (ppb)	0.0020	0.0004	25.15 ± 0.39	25.46 ± 0.60	659.6 ± 2.2	659 ± 14
Age (Ma)			139.9 ± 1.5	139.6 ± 3.8	223.0 ± 2.4	221.4 ± 5.6

†Du *et al*. (2004).
SD, Standard Deviation.

10 mL of concentrated HNO_3 and 2 mL of HCl were added. Appropriate amounts of ^{185}Re and ^{190}Os spikes were then added according to the estimated concentrations of Re and Os. The Carius tube was sealed using an oxygen-methane torch and then heated to 200°C for about 12 h. After cooling to room temperature, the Carius tube was further frozen in a refrigerator for 2 h and then opened to distill Os as OsO_4 from the matrix using in-situ distillation equipment. Rhenium was separated from the remaining solution after Os distillation using anion exchange resin (Biorad AG 1 × 8, 200–400 mesh; BioRad, Hercules, CA, USA) technique as described by Qi *et al*. (2007).

Re and Os isotopes were measured using a PE ELAN DRC-e ICP-MS in the Institute of Geochemistry, Chinese Academy of Sciences. Total blanks of Re and Os were 6.4 pg and 2.0 pg, respectively. The analytical results for molybdenite reference materials, HLP and JDC, are listed in Table 1. Iridium was added to Re and Os-bearing solution for mass discrimination correction. The calibration method was referred to Schoenberg *et al*. (2000). Measured ^{187}Os and ^{192}Os are referred to the major spike isotope ^{190}Os and are used to determine radiogenic ^{187}Os and common Os concentrations in each sample. Absolute uncertainties including uncertainties of the blank, the ^{187}Re decay constant of 1.666×10^{-11} a^{-1} (0.31%) (Smoliar *et al*., 1996), and the ^{185}Re and ^{190}Os spike calibrations (0.2%), are reported at a 2-sigma level. They were acquired by propagation of error in the calculation process using the formula of the isotopic dilution method (Alonso, 1995).

4.2 S, C, and O isotope analyses

Sulfur isotope analyses were carried out using EA-IRMS (Elemental Analysis-Isotope Ratio Mass Spectrometry) in the Institute of Geochemistry, Chinese Academy of Sciences. The elemental analyzer and isotope ratio mass spectrometry are EuroVector EA3000 and GV IsoPrime, respectively. About 130 μg pyrite powder was weighed and packed by the tinfoil. Sulfur of sulfide minerals was converted to SO_2 for isotopic analysis by burning in the reactor under a constant temperature of about 1000°C in a stream of purified oxygen. The sulfur dioxide was then carried by helium into the mass spectrometer. Sulfur isotope composition is expressed using the delta per mil notation ($\delta^{34}S$) with respect to Vienna Canyon Diablo Troilite (V-CDT). Based on repeated analyses of national standards GBW04414 (Ag_2S, $\delta^{34}S = -0.07‰$) and GBW04415 (Ag_2S, $\delta^{34}S = +22.15‰$), the precision of the analyses is better than ±0.2‰.

Carbon–oxygen isotope analyses were also carried out in the Institute of Geochemistry, Chinese Academy of Sciences. Dry sample powder of calcite was reacted with 100% H_3PO_4 at 50°C for about 3 h. After the completion of digestion, CO_2 was recovered and cryogenically trapped in liquid nitrogen traps (–195°C). All non-condensable gases produced in the reaction were pumped out to a vacuum of at least 100 mtorr. Trapped CO_2 was then cryogenically transferred to a sample flask and sealed for analysis. The trapped CO_2 was analyzed by a Finiggan MAT 252 mass spectrometer for carbon and oxygen isotope compositions. The $\delta^{13}C$ and $\delta^{18}O$ are reported with respect to Peedee Belemnite (PDB) and Standard Mean Ocean Water (SMOW), respectively. The reported values are arithmetic means of replicate analyses. The method precision monitored using national standard GBW04416 (marble, $\delta^{13}C = +1.61‰$, $\delta^{18}O = -11.59‰$) was approximately ± 0.2‰ (1σ).

5. Analytical results

5.1 Re–Os isotope of pyrite

5.1.1 Heifengshan Fe deposit

Pyrite from the Heifengshan deposit contains 29.4 to 92.3 ppb Re and 0.019 to 0.097 ppb common Os (Table 2). $^{187}Re/^{188}Os$ ratios vary widely from 1462 to

Table 2 Re–Os isotopic data for pyrite from the Heifengshan, Shuangfengshan and Shaquanzi Fe(-Cu) deposits, Eastern Tianshan Orogenic Belt

Sample no.	Mineral assemblage	Sample weight (g)	Total Re† (ppb)	2σ	^{187}Os† (ppb)	2σ	Common Os† (ppb)	2σ	^{187}Re/^{188}Os†	2σ	^{187}Os/^{188}Os†	2σ	Model age‡ (Ma)	2σ
Heifengshan Fe deposit														
HFS0904	Mag + Py + Cal	0.5069	49.7	1.6	0.159	0.010	0.022	0.006	10,633	2,594	53.0	13.2	306	22
HFS0911	Mag + Py + Cal	0.5014	29.4	2.8	0.092	0.002	0.097	0.004	1,462	142	7.0	0.2	299	30
HFS0912	Mag + Py + Cal + Chl	0.5028	39.4	0.6	0.124	0.002	0.019	0.006	10,176	3,056	50.2	15.4	301	7
HFS0913	Mag + Py + Cal	0.5075	35.1	2.0	0.110	0.002	0.070	0.008	2,426	280	11.9	1.2	299	17
HFS0914	Mag + Py	0.5084	92.3	3.8	0.295	0.006	0.030	0.004	14,903	2,124	74.5	10.4	306	14
Shuangfengshan Fe deposit														
SFS0902	Mag + Py + Cal	0.5075	103.0	3.0	0.320	0.008	0.020	0.006	24,375	7,824	118.5	38.8	297	11
SFS0903	Mag + Py + Cal	0.5075	121.2	5.2	0.374	0.014	0.016	0.004	35,422	9,246	170.9	45.2	295	17
SFS0904	Mag + Py	0.5027	141.6	5.8	0.428	0.006	0.022	0.006	30,775	7,052	145.5	33.6	289	12
SFS0908	Mag + Py	0.5022	168.9	3.8	0.516	0.016	0.014	0.006	57,526	22,462	274.6	109.6	292	11
SFS0911	Mag + Py + Cal	0.5096	20.6	1.2	0.061	0.002	0.015	0.004	6,679	1,478	30.8	6.8	283	20
SFS0912	Mag + Py + Cal	0.5072	61.0	0.6	0.187	0.008	0.013	0.008	22,463	12,088	107.6	59.2	293	13
SFS0913	Mag + Py	0.5002	184.1	2.8	0.560	0.022	0.010	0.008	84,397	67,028	401.4	325.8	291	12
Shaquanzi Fe-Cu deposit														
SQZ0920	Mag + Py + Ccp + Chl	0.5015	3.7	0.2	0.011	0.002	0.014	0.002	1,281	222	6.2	1.0	286	58
SQZ0924	Mag + Py + Ccp + Cal	0.5019	116.1	7.8	0.348	0.012	0.019	0.006	29,684	8,568	139.2	40.0	287	21
SQZ0925	Mag + Py + Ccp + Cal	0.5033	79.4	3.4	0.248	0.012	0.024	0.008	15,971	5,500	78.2	27.4	299	20
SQZ0931	Mag + Py + Ccp	0.5062	33.0	2.0	0.102	0.002	0.024	0.004	6,522	1,220	31.5	5.8	295	18
SQZ0932	Mag + Py + Ccp	0.5055	71.9	1.2	0.220	0.008	0.024	0.008	14,446	4,566	69.0	22.2	293	12
SQZ0933	Mag + Py + Ccp	0.5025	110.6	3.2	0.344	0.008	0.023	0.006	22,992	6,030	111.9	30.0	297	11

†All the data are blank corrected.
‡Model ages are calculated using the equation of $^{187}Os = {}^{187}Re\,(e^{\lambda t}-1)$, where λ (^{187}Re decay constant) = $1.666 \times 10^{-11} a^{-1}$ (Smoliar *et al.*, 1996).
Mag, magnetite; Py, pyrite; Ccp, chalcopyrite; Cal, calcite; Chl, chlorite.

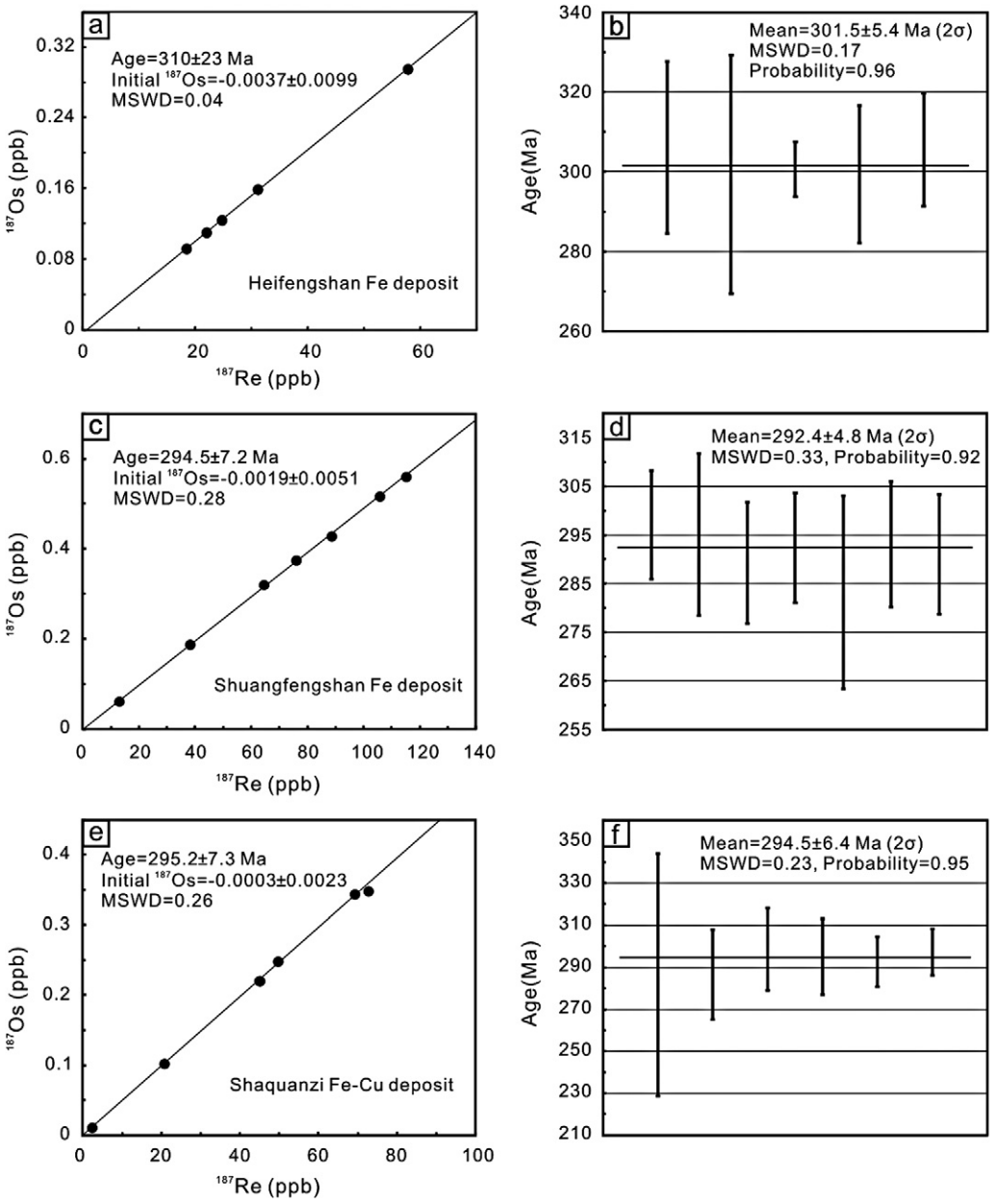

Fig. 5 ^{187}Re-^{187}Os isochron plots and diagrams of weighted mean model ages for pyrite separates from the Heifengshan (a, b), Shuangfengshan (c, d) and Shaquanzi (e, f) Fe(-Cu) deposits.

>5000, with $^{187}Os/^{188}Os$ ratios ranging from 7 to 271. Regression of the Re–Os data (n = 5) yields an isochron age of 310 ± 23 Ma (2σ, MSWD = 0.04; Fig. 5a). High $^{187}Re/^{188}Os$ ratios (>5000) in most pyrite samples allow us to calculate single mineral model ages. Analyses of five pyrite samples yield a weighted mean age of 302 ± 5 Ma (2σ) with an MSWD of 0.17 (Fig. 5b).

5.1.2 Shuangfengshan Fe deposit

The results of seven pyrite separates from the Shuangfengshan deposit are broadly similar to those from the Heifengshan deposit, having a wide range of total Re (20.6–184 ppb), but a small range of common Os (0.010–0.022 ppb). $^{187}Re/^{188}Os$ ratios vary widely from

6600 to 84400, with $^{187}Os/^{188}Os$ ratios ranging from 31 to 401. These analyses yield an isochron age of 295 ± 7 Ma (2σ, MSWD = 0.28; Fig. 5c). The weighted mean age for all pyrite separates is 292 ± 5 Ma (2 σ) with an MSWD of 0.33 (Fig. 5d), similar to the isochron age within error.

5.1.3 Shaquanzi Fe-Cu deposit

Pyrite from the Shaquanzi deposit also has highly variable Re (3.7–116.1 ppb) but relatively uniform common Os (0.014–0.024 ppb) with very high $^{187}Re/^{188}Os$ ratios ranging from 1300 to 29000. These analyses yield a ^{187}Re-^{187}Os isochron age of 295 ± 7 Ma (MSWD = 0.26; Fig. 5e) and a weighted mean model age of 295 ± 6 Ma (n = 6, MSWD = 0.23) (Fig. 5f).

5.2 Sulfur isotope

The $\delta^{34}S$ values of pyrite from three deposits are listed in Table 3, and schematically illustrated in Figure 6.

Pyrite separates from the volcanic rocks, sedimentary wall rocks, and ores in the Heifengshan Fe deposit have similar $\delta^{34}S$ values, varying narrowly from –2.6‰ to –0.41‰, with an average of –1.38‰. Similar to the Heifengshan Fe deposit, pyrite from the Shuangfengshan Fe deposit has a small range of $\delta^{34}S$ from –0.3‰ to 3.9‰ with an average of 1.78‰. In the Shaquanzi Fe–Cu deposit, pyrite from ores in open pit has different sulfur isotopes from ores in a drill core. The $\delta^{34}S$ values of most pyrite from the drill core range widely from 1.2‰ to 4.7‰, with an average of 2.4‰. Two samples, SQZ0920 and SQZ0921, from the uppermost part of the drill core have $\delta^{34}S$ values of 17.5‰ and 15.6‰, respectively, obviously different from others. The $\delta^{34}S$ values of pyrite from the open pit vary narrowly from –1.7‰ to –0.27‰, with an average of –1.17‰.

5.3 Carbon and oxygen isotope of calcite

Carbon and oxygen isotope values ($\delta^{13}C_{PDB}$; $\delta^{18}O_{SMOW}$) of calcite from the Heifengshan Fe deposit range from –2.8‰ to –1.0‰ and from 11.0‰ to 12.6‰, respectively (Table 4). Three calcite samples from the Shaquanzi Fe-Cu deposit have $\delta^{13}C_{PDB}$ (–5.5‰ to –2.3‰) and $\delta^{18}O_{SMOW}$ (10.0‰ to 12.7‰). Compared to the geological reservoirs of $\delta^{13}C_{PDB}$ and $\delta^{18}O_{SMOW}$ values (Fig. 7), $\delta^{13}C_{PDB}$ values in calcite of these two deposits are close to that of mantle CO_2 but different from atmospheric CO_2 and metamorphic CO_2 (Fig. 7a), whereas calcite from these two deposits have $\delta^{18}O_{SMOW}$ values similar to metamorphic rocks and sedimentary rocks (Fig. 7b). In the $\delta^{13}C_{PDB}$-$\delta^{18}O_{SMOW}$ diagram (Fig. 8), most calcite samples plot in the field of primary carbonates, obviously distinguishable from marine carbonates and sedimentary organism.

6. Discussion

6.1 Reliability of the Re–Os age determination

Although there is no pyrite reference material for Re–Os dating, the results for molybdenite standards, HLP and JDC, are in good agreement with the certified values, and the multiple analyses demonstrate excellent reproducibility (Table 1). The low blank level and detection limits (Table 1) ensure the accuracy of the determination of low Re and Os concentrations. Thus, the Re–Os analytical method for pyrite is reliable.

Because they have high radiogenic ^{187}Os produced by high ^{187}Re, molybdenite and some pyrite can be classified as low-level highly radiogenic (LLHR) sulfides (Stein *et al.*, 2000). LLHR sulfide minerals with $^{187}Re/^{188}Os$ ratios of ≥5000, are plotted in ^{187}Re–^{187}Os space in order to obtain accurate and meaningful ages (Stein *et al.*, 2000). Traditional $^{187}Re/^{188}Os$ (x-axis) versus $^{187}Os/^{188}Os$ (y-axis) plots may introduce highly correlated errors because low-concentration ^{188}Os has a large uncertainty. To account for this source of highly correlated uncertainty, an error correlation function has been applied to effectively assess the degree of correlation between the $^{187}Re/^{188}Os$ and $^{187}Os/^{188}Os$ ratios for a given analysis (Ludwig, 1980).

$$\rho = \frac{\left(\frac{\sigma_{(^{187}Re/^{188}Os)}}{^{187}Re/^{188}Os}\right)^2 + \left(\frac{\sigma_{(^{187}Os/^{188}Os)}}{^{187}Os/^{188}Os}\right)^2 - \left(\frac{\sigma_{(^{187}Os/^{187}Re)}}{^{187}Os/^{187}Re}\right)^2}{2 * \frac{\sigma_{(^{187}Re/^{188}Os)}}{^{187}Re/^{188}Os} * \frac{\sigma_{(^{187}Os/^{188}Os)}}{^{187}Os/^{188}Os}}$$

Where σ denotes the 1σ uncertainty (67% confidence interval) of each ratio. The error correlation coefficient ρ can be calculated for each sample by this function.

For the sample with $^{187}Re/^{188}Os$ ratios of ≥5000, the uniform error correlation coefficient ρ (about equal to 1) was acquired, suggesting that $^{187}Re/^{188}Os$ ratios are highly correlated to $^{187}Os/^{188}Os$ ratios. $^{187}Re/^{188}Os$ ratios of most pyrite separates from the Heifengshan, Shuangfengshan, and Shaquanzi Fe(-Cu) deposits are >5000 (Table 2). Thus, analytical data are plotted in ^{187}Re-^{187}Os space to obtain isochron ages using software of Isoplot version 3.23 (Ludwig, 2003).

Table 3 Sulfur isotope compositions of pyrite from the Heifengshan, Shuangfengshan and Shaquanzi Fe(-Cu) deposits, Eastern Tianshan Orogenic Belt

Heifengshan Fe deposit			Shuangfengshan Fe deposit			Shaquanzi Fe-Cu deposit		
Sample no.	Occurrence	$\delta^{34}S_{CDT}$ (‰)	Sample no.	Occurrence	$\delta^{34}S_{CDT}$ (‰)	Sample no.	Occurrence	$\delta^{34}S_{CDT}$ (‰)
HFS0903	Disseminated ore, pyrite is massive aggregate	–0.76	SFS0902	Massive ore, pyrite is euhedral crystal	0.56	SQZ0920	Massive ore from the drill core, 106 m deep, pyrite is disseminated	17.5
HFS0904	Disseminated ore, pyrite is massive aggregate	–2.1	SFS0903	Massive ore, pyrite is euhedral crystal	0.71	SQZ0921	Massive ore from the drill core, 107 m deep, pyrite is disseminated	15.6
HFS0905	Pyritized wall rock (volcanic rock), pyrite is disseminated	–1.3	SFS0904	Disseminated ore, pyrite is euhedral crystal	–0.30	SQZ0923	Disseminated ore from the drill core, 113 m deep, pyrite is euhedral crystal	2.0
HFS0906	Banded ore, pyrite is euhedral crystal	–1.2	SFS0905	Disseminated ore, pyrite is euhedral crystal	2.7	SQZ0924	Disseminated ore from the drill core, 114 m deep, pyrite is euhedral crystal	1.7
HFS0907	Pyritized wall rock (sedimentary), pyrite is euhedral crystal	–1.4	SFS0908	Disseminated ore, pyrite is euhedral crystal	2.9	SQZ0925	Massive ore from the drill core, 115 m deep, pyrite is disseminated	4.7
HFS0911	Disseminated ore, pyrite is massive aggregate	–1.8	SFS0911	Disseminated ore, pyrite is euhedral crystal	3.9	SQZ0928	Massive ore from the drill core, 117 m deep, pyrite is disseminated	1.2
HFS0912	Massive ore, pyrite is euhedral crystal	–0.85	SFS0912	Massive ore, pyrite is euhedral crystal	2.5	SQZ0931	Massive ore from the open pit, pyrite is disseminated	–1.7
HFS0913	Massive ore, pyrite is euhedral crystal	–2.6	SFS0913	Disseminated ore, pyrite is massive aggregate	2.9	SQZ0932	Massive ore from the open pit, pyrite is disseminated	–0.92
HFS0914	Pyritized wall rock (volcanic rock), pyrite is massive aggregate	–0.41	SFS0914	Disseminated ore, pyrite is euhedral crystal	0.15	SQZ0933	Massive ore from the open pit, pyrite is disseminated	–0.88
						SQZ0936	Massive ore from the open pit, pyrite is disseminated	–0.27

For the LLHR sulfide minerals, the Re–Os ages of these minerals can be calculated directly from ^{187}Re and ^{187}Os concentrations (Stein *et al*., 2000). Because most pyrite separates from the Fe(-Cu) deposits in Eastern Tianshan have relatively high Re and low common Os, the ages thus can be calculated essentially in the same manner as molybdenite. Weighted mean ages can be calculated assuming that there is no external error by software of Isoplot version 3.23 (Ludwig, 2003).

The weighted mean ages of the Heifengshan, Shuangfengshan, and Shaquanzi Fe(-Cu) deposits are identical to their isochron ages within uncertainties, demonstrating the reliability of the ages. Because the error of the weighted mean age is smaller than that of the isochron age, the weighted mean age is chosen in this study to represent the age of pyrite formation.

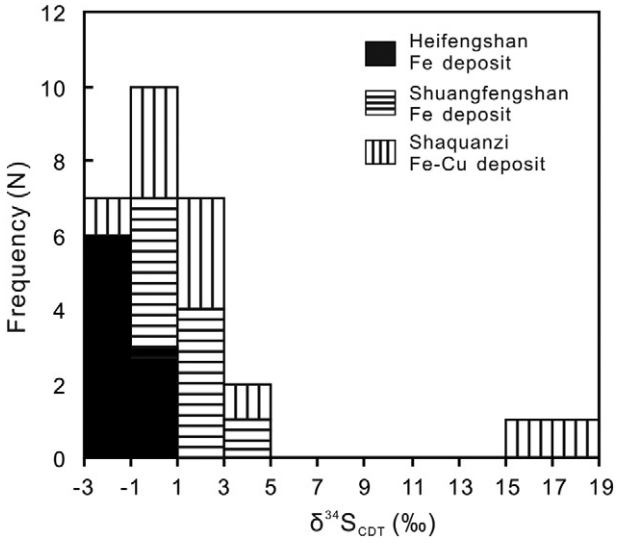

Fig. 6 Histogram of sulfur isotope compositions of pyrite from the Heifengshan, Shuanfengshan and Shaquanzi Fe(-Cu) deposits.

6.2 Rhenium of pyrite and its significance

Pyrite separates from the Heifengshan, Shuangfengshan, and Shaquanzi Fe(-Cu) deposits have a wide range of Re from 3.7 to 184 ppb (Table 2), similar to that of pyrite from other deposits in the world (Fig. 9). However, magnetite from these three deposits has low Re content (<1 ppb). What controls Re contents of pyrite remains unresolved due to the complex behavior of Re in the mineral system.

Pyrite usually has Re contents of ppb level, lower than that of molybdenite (ppm level), but usually higher than silicate and oxide minerals (ppt level) (Davies, 2010). The relatively high Re contents of pyrite suggest that pyrite, like many other sulfides, acts as an efficient Re sink as it is capable of preferentially taking up large quantities of Re from the ore-forming fluids. Fe^{2+}-bearing minerals such as pyrite and pyrrhotite may act as efficient redox partners according to the following redox reaction: $2Fe^{2+} + Re^{6+} = 2Fe^{3+} + Re^{4+}$ (Frei *et al*., 1998). However, the wide ranges of Re of pyrite from the same sample suggest that the distribution of Re is not controlled by crystallographic structure (Freydier *et al*., 1997; Stein *et al*., 1998). Selby *et al*. (2009) thought that Re–Os budget in the sulfides could be controlled by microintergrowths of molybdenite in sulfides from the carbonate-hosted copper deposits at Ruby Creek. Due to similar geochemical behaviors of Mo and Re and affinity of Re with Ge-bearing minerals, it is thought that Re is predominantly hosted in the intergrowths of germanite and renierite in sulfides of Ruby Creek (Selby *et al*., 2009). Strong correlations of

Table 4 Carbon and oxygen isotope compositions of calcite from the Heifengshan Fe deposit and Shaquanzi Fe-Cu deposit, Eastern Tianshan Orogenic Belt

Sample no.	Occurrence	$\delta^{13}C_{PDB}$ (‰)	$\delta^{18}O_{SMOW}$ (‰)
Heifengshan Fe deposit			
HFS0901	Massive ore, calcite is lump	–1.3	11.4
HFS0903	Disseminated ore, calcite is lump	–1.3	12.6
HFS0904	Disseminated ore, calcite is lump	–2.8	12.1
HFS0911	Disseminated ore, calcite is lump	–2.0	12.1
HFS0912	Massive ore, calcite is lump	–1.0	11.0
HFS0913	Massive ore, calcite is lump	–2.1	11.9
Shaquanzi Fe-Cu deposit			
SQZ0923	Disseminated ore, calcite is granulate	–5.5	12.7
SQZ0924	Disseminated ore, calcite is granulate	–2.3	10.0
SQZ0925	Massive ore, calcite is granulate	–2.4	10.0

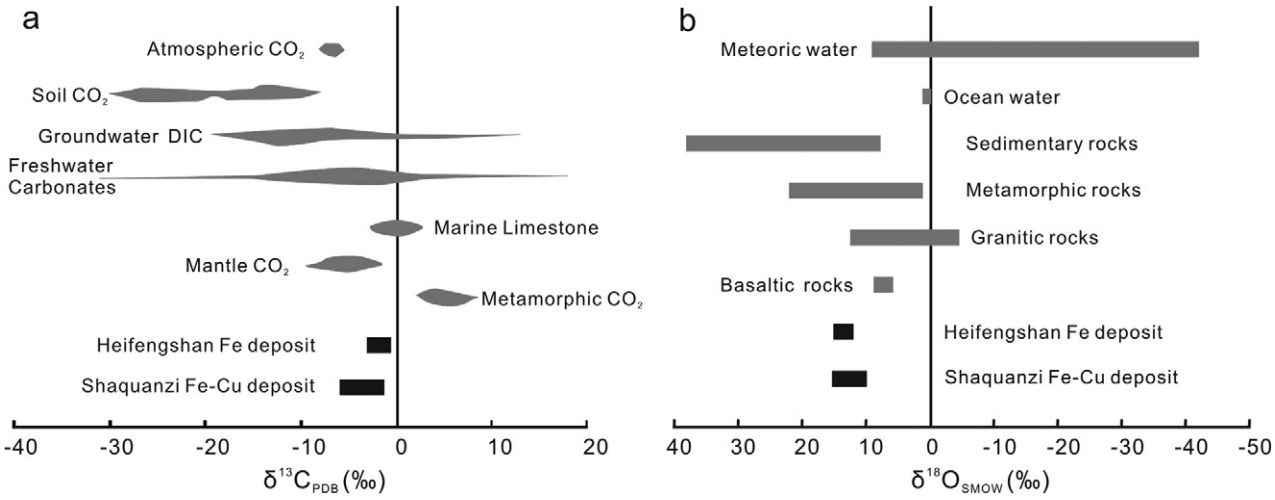

Fig. 7 $\delta^{13}C_{PDB}$ (a; after Clark & Fritz, 1997) and $\delta^{18}O_{SMOW}$ (b; after Hoefs, 1997) values of representative geological reservoirs.

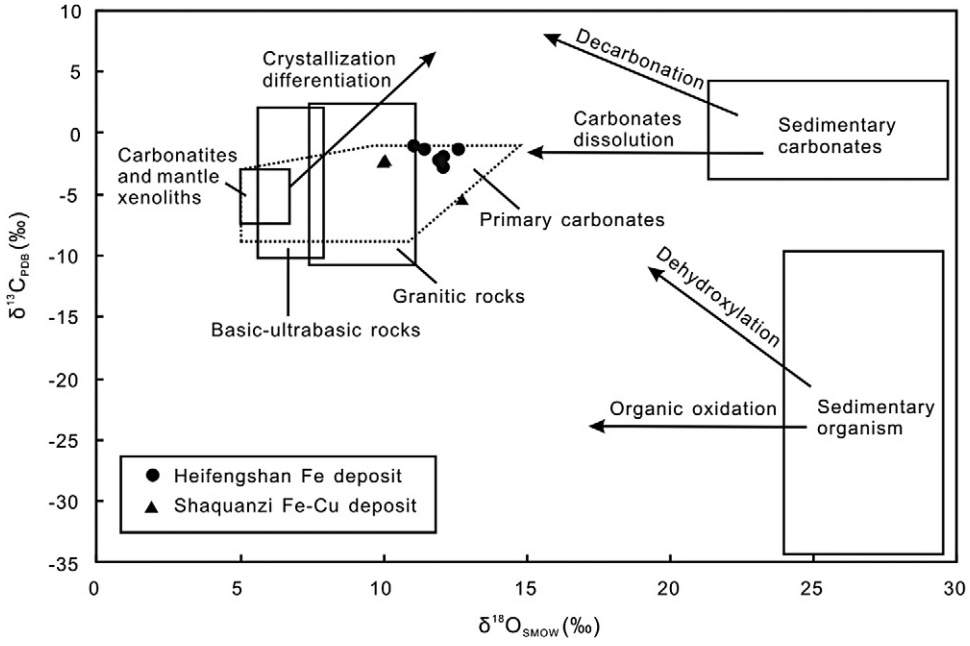

Fig. 8 $\delta^{13}C_{PDB}$-$\delta^{18}O_{SMOW}$ diagram of calcite in ores from the Heifengshan Fe deposit and Shaquanzi Fe-Cu deposit (modified from Liu and Liu, 1997, Liu *et al*., 2003).

Re with Co, Ni, Cu, and Ge support this conclusion (Selby *et al*., 2009).

On the other hand, pyrite associated with Cu/Fe-rich minerals has relatively high Re, whereas pyrite associated with W/Pb/Zn/Au/Ag-rich minerals has relatively low Re. Re contents of pyrite vary widely in different types of deposits, but there are certain patterns. For example, pyrite from Au deposits (Kirk *et al*., 2001; Chen *et al*., 2007; Kerr & Selby, 2012) or Au–Cu deposits (Stein *et al*., 1998; Arne *et al*., 2001) has relatively low Re, ranging from 0.022 to 26 ppb (mostly ~5 ppb) (Fig. 9). Pyrite from Cu–Au deposits (Cardon *et al*., 2008; Xie *et al*., 2009; Guo *et al*., 2011) or Cu–Ag deposits (Selby *et al*., 2009) has relatively high Re (Fig. 9). Pyrite from Fe deposits (this study) or Fe–Cu deposits (Mathur *et al*., 1999; Morgan *et al*., 2000)

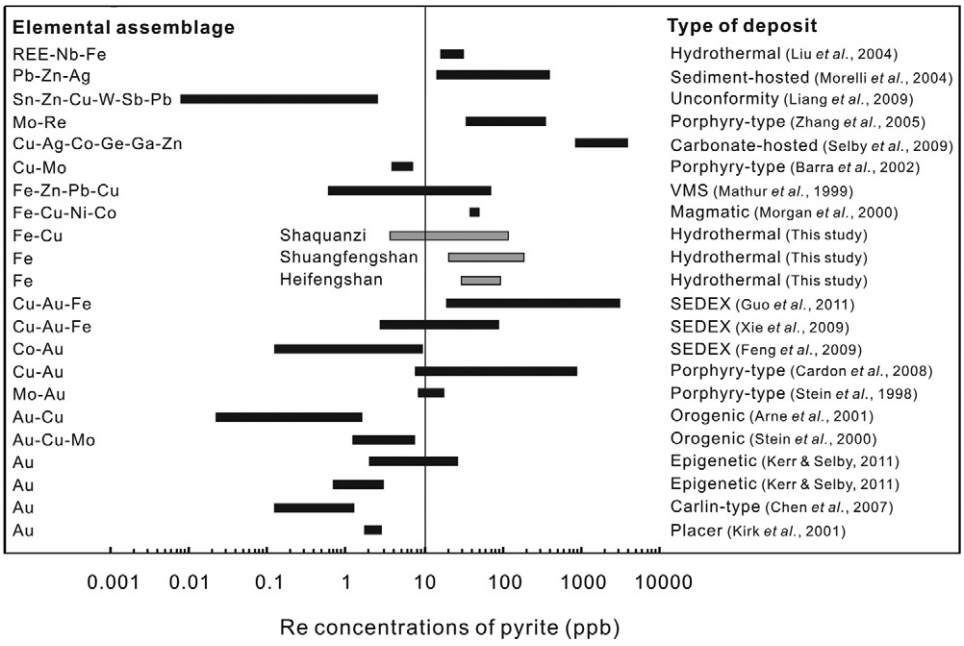

Fig. 9 Correlation diagram of Re concentrations of pyrite, elemental assemblages and types of deposit.

usually has moderate Re (Fig. 9). Moreover, numerous data from our Re–Os isotope laboratory suggest that pyrite from W–Sn deposits and Pb–Zn deposits usually has very low Re content (mostly <1 ppb). This phenomenon was also observed in molybdenite according to Yang *et al*. (2011). Yang *et al*. (2011) reported the highest Re content of molybdenite associated with chalcopyrite and/or pyrite, pyrrhotite, magnetite, whereas molybdenite associated with scheelite (wolframite) and/or galena, sphalerite, native gold, and native silver has the lowest Re content. Zhang *et al*. (2005) also thought that high-temperature mineral assemblages (i.e. quartz–molybdenite–chalcopyrite) usually had high Re content. Therefore, we can conclude that Re would be enriched in the Cu/Fe-bearing fluids but depleted in W/Pb/Zn/Au/Ag-bearing fluids.

In the Heifengshan, Shuangfengshan and Shaquanzi Fe(-Cu) deposits, sulfide minerals do not contain molybdenite. Both pyrite separates and bulk ores have very low Mo (<1 ppm). Therefore, it is impossible to have microintergrowths of molybdenite to explain the relatively high Re content of pyrite. The characteristic mineral assemblage (magnetite + pyrite +/− chalcopyrite) may be tracers for the pyrite of relatively high Re content. The magma-related ore-forming fluid may be the main controlling factor for the relatively high Re content in pyrite of this study.

6.3 Time of formation of Fe(-Cu) deposits in the ETOB

Although numerous studies of the Heifengshan, Shuangfengshan, and Shaquanzi Fe(-Cu) deposits are available (Song *et al*., 1983; He *et al*., 1994a; Jiang *et al*., 2002; Xiao, 2003; Fang *et al*., 2006a, b; Wang *et al*., 2006b), the ore genesis remains a matter of debate, due to the lack of precise mineralization ages.

The Fe(-Cu) deposits in the Aqishan–Yamansu belt were previously suggested to have formed during Early Carboniferous on the basis of sericite K–Ar ages of c. 350 Ma (Liu *et al*., 1996). In the Yamansu Fe deposit, west of the belt, wall rock andesitic porphyry has a whole-rock Rb–Sr isochron age of 374 ± 44 Ma, while garnet-epidote has a mineral Sm–Nd isochron age of 352 ± 46 Ma, which were thought to represent the timing of volcanic eruption and mineralization, respectively (Li & Chen, 2003). However, these ages have large errors and their conclusion is thus questionable. SHRIMP zircon U-Pb dating of diorite porphyry yielded an age of c. 290 Ma (Li & Liu, 2003), much younger than previously thought. Moreover, the Bailingshan skarn Fe(-Cu) deposit in the belt has a Late Carboniferous to Early Permian Rb-Sr age of 286 ± 12 Ma for ore-bearing quartz veins (Li & Liu, 2003), thus, inconsistent with early Carboniferous mineralization.

Our precise Re–Os ages of pyrite for the first time provide important constraints on the timing of the Fe(-Cu) deposits. The Heifengshan, Shuangfengshan, and Shaquanzi Fe(-Cu) deposits have similar mineralization ages ranging from c. 292–302 Ma with small uncertainties and are believed to have formed at the same time. If we combine all the data together, an average age of ~296 Ma is obtained. The ~296 Ma Fe(-Cu) deposits are obviously younger than the early to middle Carboniferous host volcanic rocks, suggesting the Fe(-Cu) deposits were not related to the early to middle Carboniferous volcanism as previously suggested.

6.4 Possible origin of Fe(-Cu) deposits in the ETOB

The origin of the Fe-(Cu) deposits in Eastern Tianshan is still controversial. These deposits have been thought to be skarn type because of their close association with felsic intrusions (Song, 1985). They have also been thought to be typical volcanic-hydrothermal deposits (Song *et al*., 1983), ore slurry eruption-injection deposits (He *et al*., 1994a), contact metamorphic volcanogenic-sedimentary deposits (Jiang *et al*., 2002), and sedimentary exhalative deposits (SEDEX) (Wang *et al*., 2006b), because the Fe(-Cu) deposits are hosted in the strata of volcanic rocks or volcanoclastic rocks.

Our sulfur isotope compositions of pyrite, and the carbon and oxygen isotope compositions of calcite provide significant constraints on the origin of these Fe(-Cu) deposits. Pyrite is the predominant sulfide phase in the Heifengshan, Shuangfengshan, and Shaquanzi Fe(-Cu) deposits, thus, the sulfur composition of pyrite can represent the sulfur composition of total sulfur in the ore-forming fluids (Kajiwara, 1971). The near zero sulfur isotope compositions of pyrite from these Fe(-Cu) deposits indicate that S of the ore-forming fluids were mantle-derived. The characteristic sulfur might have been derived either directly from partial melting that produced the magmatic fluids or through dissolution and leaching of pre-existing sulfide-bearing igneous sources (Ohmoto, 1972). Anhydrite from the country rocks has the $\delta^{34}S$ values ranging from 13.1‰ to 17.9‰ (Song, 1985), close to Pennsylvania seawater sulfate (14‰ to 14.7‰), showing that the seawater sulfate is usually enriched in heavy sulfur. Two pyrite samples (SQZ0920 and SQZ0921) from the upper part of the drill core in the Shaquanzi Fe–Cu deposit are enriched in heavy sulfur (Fig. 6), probably due to the addition of the sulfur from crustal anhydrite.

Three end members can be the source of carbon in hydrothermal system (Fig. 8), including: (i) mantle degasification and magmatic source with $\delta^{13}C$ values ranging from −9‰ to −2‰. Carbon isotope fractionation generally decreases with increasing temperature and it becomes fairly small at high temperature (Clark & Fritz, 1997); (ii) sedimentary carbonates, with $\delta^{13}C$ values from −2‰ to +3‰; (iii) sedimentary organism, which is usually extremely enriched in ^{12}C with $\delta^{13}C$ values from −30‰ to −15‰. Carbon isotope compositions of calcite from the Heifengshan Fe deposit and Shaquanzi Fe–Cu deposit are similar to those of mantle CO_2 and freshwater carbonates, different from atmospheric CO_2 and metamorphic CO_2 (Fig. 7a).

Oxygen isotope compositions of calcite from these two deposits are within the range of sedimentary and metamorphic rocks, but beyond the range of meteoric and ocean waters (Fig. 7b). Most $\delta^{13}C$ and $\delta^{18}O$ values of calcite from these deposits plot in the field of primary carbonates, obviously away from the field of marine carbonates and sedimentary organisms and their evolutionary products (Fig. 8). Therefore, C and O suggest a magmatic-hydrothermal origin.

Sulfur isotope of pyrite and C-O isotope of calcite from these Fe(-Cu) deposits suggest that S, C, and O are mantle-derived. Therefore, the formation of these deposits was likely to be related to the ~296 Ma mantle-derived magmatism.

The Heifengshan, Shuangfengshan, and Shaquanzi Fe(-Cu) deposits have similar mineral assemblages and hydrothermal alteration. Their ores contain low-Ti magnetite (usually <0.5 wt.% TiO_2) and Fe/Cu-sulfides, different from SEDEX ores which are dominated by Fe/Cu-sulfides (Pirajno, 2009). These three deposits contain Cu, Au, and REE, as by-products with 274–1194 ppm Cu, 20–180 ppb Au, and 29.7–36.3 ppm total REE. In addition, these deposits are structurally controlled and the ore bodies distribute along the Shaquanzi fault. These mineralization styles are comparable to those of major Iron-Oxide-Copper-Gold (IOCG) deposits elsewhere in the world. For example, IOCG deposits in the Candelaria-Punta del Cobre area, Chile (Marschik and Fontboté, 2001), and in the Tennant Creek and Cloncurry districts, Australia (e.g. Huston *et al*., 1993; Baker, 1998) contain abundant hydrothermal low-Ti magnetite and/or hematite and Cu-sulfides with REE, Mo, Au, Ag, U, Co, and F as by-products, accompanied by extensive Na–K–Ca alteration and are strongly structurally controlled. Therefore, the mineralization styles of the

Heifengshan, Shuangfengshan, and Shaquanzi Fe(-Cu) deposits may suggest a possible IOCG metallogenic province in Eastern Tianshan.

6.5 Implications for the regional mineralization

Several models have been proposed for the regional mineralization of the ETOB (Feng *et al*., 2002; Mao *et al*., 2002a, 2005; Zhang *et al*., 2004, 2008), but the ore-forming processes of the Fe(-Cu) deposits were not sufficiently discussed. The Paleozoic geological evolution of the ETOB involved subduction of oceanic slab and collision of arcs (Windley *et al*., 1990; Allen *et al*., 1993; He *et al*., 1994b; Carroll *et al*., 1995; Ma *et al*., 1997; Gao *et al*., 1998; Xiao *et al*., 2004). Mineralization in the ETOB occurred mainly in the following four stages.

The first stage of mineralization was from the Devonian to Early Carboniferous, the North Tianshan ocean was subducted beneath the Dananhu–Tousuquan (Ordovician-Silurian?) island arc (Fig. 10a), forming Devonian arc volcanic rocks and the Kanggurtag accretionary wedge.

From the Early to Middle Carboniferous (Fig. 10b), N-dipping subduction beneath the Dananhu–Tousuquan arc may have caused the back-arc extension, forming the Aqishan–Yamansu rift zone. Large volumes of Carboniferous intra-plate rift-related volcanic rocks with ages of c. 354–319 Ma were produced in the Aqishan–Yamansu zone (Xiao *et al*., 1992; Qin *et al*., 2002; Xia *et al*., 2003, 2008b), suggesting the existence of this early Carboniferous rift zone. The arc magmatism has produced porphyry Cu deposits, including the well-known Tuwu and Yandong deposits (Rui *et al*., 2002; Zhang *et al*., 2006).

During the Late Carboniferous (Fig. 10c), continent–continent and arc–continent collisions resulted in ductile deformation and thrusting (Zhang *et al*., 2008). Associated with this was the formation of orogenic-type gold deposits, and also the emplacement of igneous intrusions in the Aqishan–Yamansu rift belt and the northern margin of the Central Tianshan belt. Hydrothermal activities associated with this magmatism resulted in extensive alteration of Carboniferous volcanic rocks and volcanoclastic rocks and the formation of the IOCG-type deposits hosted in Carboniferous rift-related volcanic rocks along major faults in the TOB. These IOCG deposits may define an IOCG metallogenic belt in the region.

From the Latest Carboniferous to Permian, post-collisional extensional events are dominant in Eastern Tianshan (Fig. 10d). Numerous mafic-ultramafic intrusions (300–270 Ma) were emplaced along the eastern section of the Kanggurtag belt (Qin *et al*., 2003b; Han *et al*., 2004; Zhou *et al*., 2004; Wu *et al*., 2005). In addition, c. 285 Ma granitic magmatism is thought to have formed the Tarim Large Igneous Province (Zhou *et al*., 2009). The mafic and granitic intrusions were thought to have formed by the plume-related activity within a continental setting following the Carboniferous amalgamation of arc-related belts in the Central Asian Orogenic Belt (Zhou *et al*., 2004). The deposits in this stage were dominated by magmatic Cu–Ni sulfide deposits and Fe-V-Ti oxide deposits. Some hydrothermal deposits also have formed in this stage, including hydrothermal vein-type Cu deposits and Cu–Ag–Pb–Zn deposits.

7. Conclusions

Pyrite separates of ores from the Heifengshan, Shuangfengshan, and Shaquanzi Fe(-Cu) deposits have relatively high and variable Re ranging from 3.7 to 184 ppb. The characteristic mineral assemblage (magnetite + pyrite ± chalcopyrite) may be tracers for the pyrite of relatively high Re content. The magma-related ore-forming fluids rather than the microintergrowths in pyrite control Re content in pyrite. Pyrites from these three deposits have similar Re–Os ages of ~296 Ma. Sulfur isotope of pyrite and carbon-oxygen isotope of calcite indicate that S, C, and O of these deposits are magmatic-hydrothermal in origin. According to the regional tectonic evolution of ETOB, we suggest that the Heifengshan, Shuangfengshan, and Shaquanzi Fe(-Cu) deposits were closely related to Late Carboniferous rift magmatism in a back-arc extensional environment. Identification of IOCG deposits may be a new target for Fe(-Cu) exploration in the TOB.

Acknowledgments

This study was financially supported by the Chinese 973 project (2012CB416804), the "CAS Hundred Talents" Project from the Chinese Academy of Sciences (KZCX2-YW-BR-09) to Qi Liang, and the National Natural Science Foundation of China (NSFC40773070). Field work was assisted by Deng Gang from No.6 Geological Team of Xinjiang. We are grateful to Prof. Huang Zhilong from the Institute of Geochemistry, CAS and Yang Shenhong, Liu Pingping, Zhao

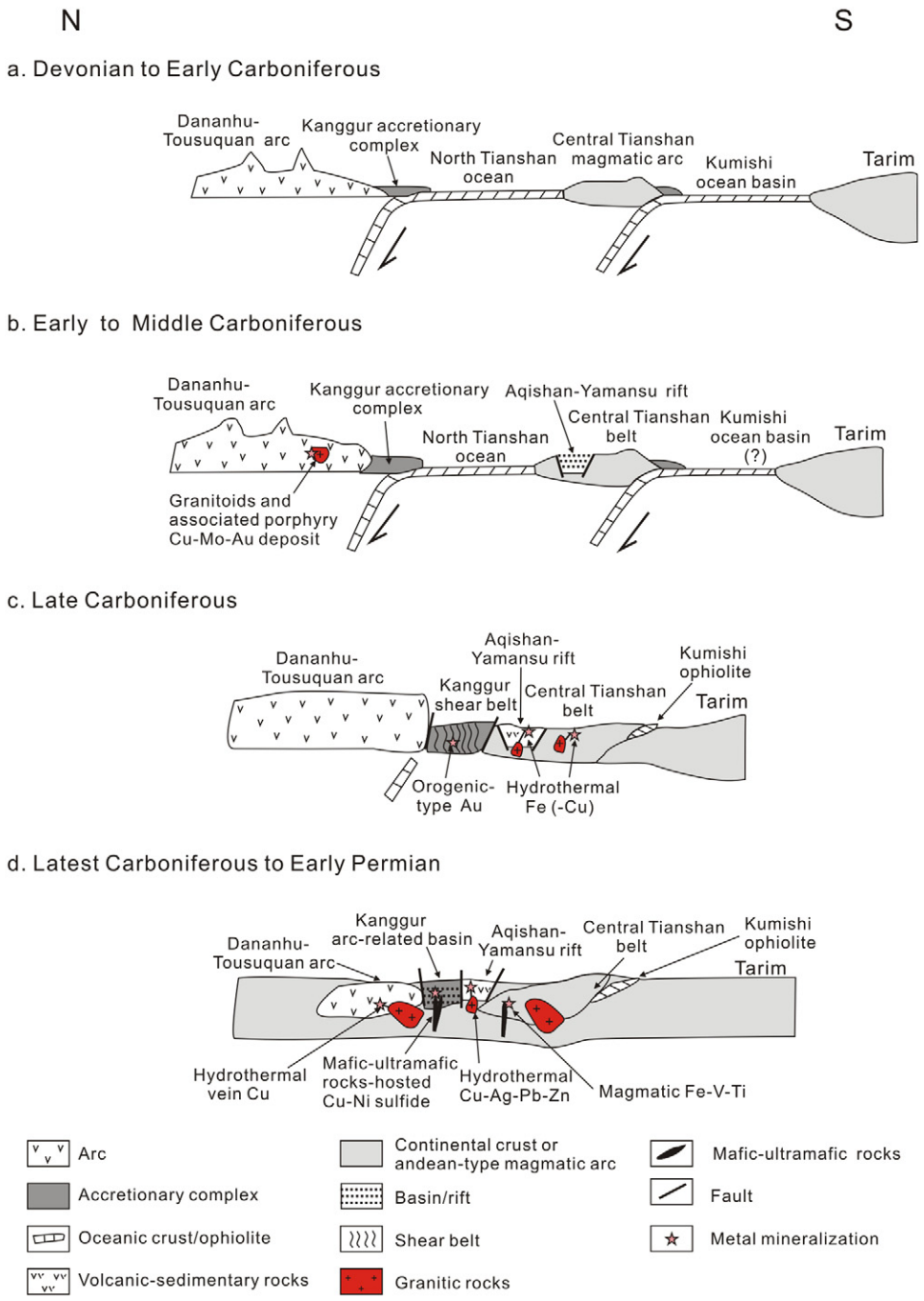

Fig. 10 Late Paleozoic tectonic evolution and related mineralization for Eastern Tianshan, modified after Xiao *et al*. (2004), Mao *et al*. (2005) and Zhang *et al*. (2008).

Xinfu, Chen Wei, and Wang Wei from the University of Hong Kong for fruitful discussion. We are very grateful to Dr. Tatsuo Nozaki and Dr. Yasushi Watanabe for careful reviews and valuable comments.

References

Allen, M., Windley, B. and Zhang, C. (1993) Palaeozoic collisional tectonics and magmatism of the Chinese Tien Shan, central Asia. Tectonophysics, 220, 89–115.

Alonso, J. (1995) Determination of fission products and actinides by inductively coupled plasma-mass spectrometry using isotope dilution analysis: a study of random and systematic errors. Anal. Chim. Acta, 312, 57–78.

Arne, D. C., Bierlin, F. P., Morgan, J. W. and Stein, H. J. (2001) Re–Os dating of sulfides associated with gold mineralization in central Victoria, Australia. Econ. Geol., 96, 1455–1459.

Baker, T. (1998) Alteration, mineralization, and fluid evolution at the Eloise Cu-Au deposit, Cloncurry District, northwest Queensland, Australia. Econ. Geol., 93, 1213–1236.

Barra, F., Ruiz, J., Mathur, R. and Titley, S. (2002) A Re–Os study of sulfide minerals from the Bagdad porphyry Cu-Mo deposit, northern Arizona, USA. Miner. Deposita, 38, 585–596.

Brenan, J. M., Cherniak, D. J. and Rose, L. A. (2000) Diffusion of osmium in pyrrhotite and pyrite: implications for closure of the Re–Os isotopic system. Earth Planet. Sci. Lett., 180, 399–413.

Cardon, O., Reisberg, L., Andre-Mayer, A. S., Leroy, J., Milu, V. and Zimmermann, C. (2008) Re–Os systematics of pyrite from the Bolcana porphyry copper deposit, Apuseni mountains, Romania. Econ. Geol., 103, 1695–1702.

Carroll, A. R., Graham, S. A., Hendrix, M. S., Ying, D. and Zhou, D. (1995) Late Paleozoic tectonic amalgamation of northwestern China: sedimentary record of the northern Tarim, northwestern Turpan, and southern Junggar basins. Geol. Soc. Am. Bull., 107, 571–594.

Che, Z. C., Liu, H. F. and Liu, L. (1994) The formation of evolution of central Tianshan Orogenic Belt. Geological Publishing House, Beijing, 1–135 (in Chinese).

Chen, M. H., Mao, J. W., Qu, W. J., Wu, L. L., Uttley, P. J., Norman, T., Zheng, J. M. and Qin, Y. Z. (2007) Re–Os dating of arsenian pyrites from the Lannigou gold deposit, Zhenfeng, Guizhou province, and its geological significances. Geol. Rev., 53, 371–382 (in Chinese with English abstract).

Chen, S. P. (2006) Study on mineralization regularity and mineral resource assesment in Hami, Xinjiang. Chinese Academy of Geological Sciences, Beijing, 1–159 (in Chinese).

Chen, S. P., Wang, D. H., Qu, W. J., Chen, Z. H. and Gao, X. L. (2005) Geological features and ore formation of the Hulu Cu-Ni sulfide deposit, Eastern Tianshan, Xinjiang. Xinjiang Geol., 23, 230–233 (in Chinese with English abstract).

Clark, I. and Fritz, P. (1997) Environmental isotopes in hydrogeology. Lewis Pubisher, New York, 328p.

Davies, J. (2010) Re–Os geochronology of oxide minerals. University of Alberta, Edmonton, 1–155.

Du, A. D., Wu, S. Q., Sun, D. Z., Wang, S. X., Qu, W. J., Markey, R., Stein, H., Morgan, J. and Malinovskiy, D. (2004) Preparation and certification of Re–Os dating reference materials: molybdenites HLP and JDC. Geostand. Geoanal. Res., 28, 41–52.

Fang, W. X., Gao, Z. Q., Jia, R. X., Huang, Z. Y., Liu, Z. T., Li, F. S., and Xu, G. D. (2006a) Geological exploration potentials and geochemical study on rocks and ores in Shaquanzi copper and copper-iron deposits, east Xinjiang. Acta Petrol. Sin., 22, 1413–1424 (in Chinese with English abstract).

Fang, W. X., Huang, Z. Y., Tang, H. F. and Gao, Z. Q. (2006b) Lithofacies, geological and geochemical characteristics and tectonic setting of Late Carboniferous volcanic-sedimentary rocks in the Kumtag-Shaquanzi area, East Tianshan. Chin. Geol., 33, 529–544 (in Chinese with English abstract).

Feng, C. Y., Qu, W. J., Zhang, D. Q., Dang, X. Y., Du, A. D., Li, D. X. and She, H. Q. (2009) Re–Os dating of pyrite from the Tuolugou stratabound Co(Au) deposit, eastern Kunlun Orogenic Belt, northwestern China. Ore Geol. Rev., 36, 213–220.

Feng, Y. M., Zhu, B. Q., Yang, J. L. and Zhang, K. C. (2002) Tectonics and evolution of the eastern Tianshan mountains-a brief introduction to" tectonic map (1:500000) of the eastern Tianshan Mountains of Xinjiang. Xinjiang Geol., 20, 309–314 (in Chinese with English abstract).

Frei, R., Nägler, T. F., Schönberg, R. and Kramers, J. D. (1998) Re–Os, Sm-Nd, U-Pb, and stepwise lead leaching isotope systematics in shear-zone hosted gold mineralization: genetic tracing and age constraints of crustal hydrothermal activity. Geochim. Cosmochim. Acta, 62, 1925–1936.

Freydier, C., Ruiz, J., Chesley, J., McCandless, T. and Munizaga, F. (1997) Re–Os isotope systematics of sulfides from felsic igneous rocks: application to base metal porphyry mineralization in Chile. Geology, 25, 775–778.

Gao, J., Li, M. S., Xiao, X. C., Tang, Y. Q. and He, G. Q. (1998) Paleozoic tectonic evolution of the Tianshan Orogen, northwestern China. Tectonophysics, 287, 213–231.

Gao, Z. J., Chen, J. X. and Lu, S. N. (1993) Precambrian geology of northern Xinjiang. Geological Publishing House, Beijing, 1–171 (in Chinese).

Guo, W. M., Lu, J. J., Jiang, S. Y., Zhang, R. Q. and Qi, L. (2011) Re–Os isotope dating of pyrite from the footwall mineralization zone of the Xinqiao deposit, Tongling, Anhui Province: geochronological evidence for submarine exhalative sedimentation. Chin. Sci. Bull., 56, 1–6.

Han, B. F., Ji, J. Q., Song, B., Chen, L. H. and Li, Z. H. (2004) SHRIMP zircon U-Pb ages of Kalatongke No. 1 and Huangshandong Cu-Ni-bearing mafic-ultramafic complexes, North Xinjiang, and geological implications. Chin. Sci. Bull., 49, 2424–2429 (in Chinese with English abstract).

Han, C. M., Xiao, W. J., Zhao, G. C., Ao, S. J., Zhang, J. E., Qu, W. J. and Du, A. D. (2010) In-Situ U-Pb, Hf and Re–Os isotopic analyses of the Xiangshan Ni-Cu-Co deposit in Eastern Tianshan (Xinjiang), Central Asia Orogenic Belt: constraints on the timing and genesis of the mineralization. Lithos, 120, 547–562.

He, D. L., Zhou, J. Y. and Mao, Y. S. (1994a) Occurrence and metallogenic mechanism of volcanic-type iron deposits in eastern Tianshan mountain. Geol. Sci. Xinjiang, 5, 41–53 (in Chinese with English abstract).

He, G. Q., Li, M. S. and Liu, D. Q. (1994b) Paleozoic crustal evolution and mineralization in Xinjiang of China. Xinjiang People's Publishing House, Urimqi, 62–245 (in Chinese).

Hoefs, J. (1997) Stable isotope geochemistry. Springer, Heidelberg, 1–201.

Hua, L. B. (2001) Element geochemistry subarea and ore-finding direction of metallogenic district, Yamansu-Shaquanzi, eastern Tianshan, Xinjiang. J. Guilin Inst. Technol., 21, 99–103 (in Chinese with English abstract).

Hua, L. B., Yang, X. and Zhong, H. (2002) Geochemical characteristics and ore-finding forecast of " 'shaquanzi' " area, eastern Tianshan, Xinjiang. Miner. Resour. Geol., 16, 291–296 (in Chinese with English abstract).

Huston, D. L., Bolger, C. and Cozens, G. (1993) A comparison of mineral deposits at the Gecko and White Devil deposits; implications for ore genesis in the Tennant Creek District, Northern Territory, Australia. Econ. Geol., 88, 1198–1225.

Ji, J. S., Tao, H. X., Zeng, Z. R., Yang, X. K. and Zhang, L. C. (1994) Geology and mineralization of the Kangurtag gold belt in

Eastern Tianshan. Geological Publishing House, Beijing, 1–20 (in Chinese).
Jiang, F. Z., Qin, K. Z., Fang, T. H. and Wang, S. L. (2002) Types, geological characteristics, metallogenic regularity and exploration target of iron deposits in eastern Tianshan mountains. Xinjiang Geol., 20, 379–383 (in Chinese with English abstract).
Kajiwara, Y. (1971) Sulfur isotope study of the Kuroko-ores of the Shakanai No. l deposits, Akita Prefecture, Japan. Geochem. J., 4, 157–181.
Kerr, A. and Selby, D. (2012) The timing of epigenetic gold mineralization on the Baie Verte Peninsula, Newfoundland, Canada: new evidence from Re–Os pyrite geochronology. Miner. Deposita, 47, 325–337.
Kirk, J., Ruiz, J., Chesley, J., Titley, S. and Walshe, J. (2001) A detrital model for the origin of gold and sulfides in the Witwatersrand basin based on Re–Os isotopes. Geochim. Cosmochim. Acta, 65, 2149–2159.
Li, H. Q. and Chen, F. W. (2003) Isotopic geochronology of regional mineralization in Xinjiang, NW. China. Geological Publishing House, Beijing (in Chinese).
Li, H. Q. and Liu, D. Q. (2003) Newsletter of Research Project of Exploration and Assessment for Xinjiang Mineral Resources, Urumqi, 6p. (in Chinese).
Li, H. Q., Xie, C. F. and Chang, H. L. (1998) Study on metallogenic chronology of nonferrous and precious metallic ore deposits in northern Xinjiang, China. Geological Publication House, Beijing, 1–263 (in Chinese).
Liang, T., Wang, D. H., Qu, W. J., Cai, M. H. and Wei, K. L. (2009) Re–Os isotope composition and source of ore-forming material of pytite in Tongkeng tin-pollmetallic deposit, Guangxi. J. Earth Sci. Environ., 31, 230–235 (in Chinese with English abstract).
Liu, D. Q., Tang, Y. L. and Zhou, R. H. (1996) Metallogenic series types of deposits in Xinjiang. Miner. Depos., 15, 207–215 (in Chinese with English abstract).
Liu, J. M. and Liu, J. J. (1997) Basin fluid genetic model of sediment-hosted micro-disseminated gold deposits in the gold-triangle area between Guizhou, Guangxi and Yunnan. Acta Miner. Sin., 17, 448–456 (in Chinese with English abstract).
Liu, J. M., Ye, J., Xu, J. H., Sun, J. G. and Shen, K. (2003) C-O and Sr-Nd isotopic geochemistry of carbonates minerals from gold deposits in East Shandong, China. Acta Petrol. Sin., 19, 775–784 (in Chinese with English abstract).
Liu, Y., Yang, G., Chen, J., Du, A. and Xie, Z. (2004) Re–Os dating of pyrite from Giant Bayan Obo REE-Nb-Fe deposit. Chin. Sci. Bull., 49, 2627–2631.
Ludwig, K. R. (1980) Calculation of uncertainties of U-Pb isotope data. Earth Planet. Sci. Lett., 46, 212–220.
Ludwig, K. R. (2003) A geochronological toolkit for Microsoft Excel. Berkeley Geochronology Center Special Publication No. 4, 1–70.
Ma, R. S., Wang, C. Y. and Ye, S. F. (1993) Tectonic framework and crust evolution of Eastern Tianshan. Nanjing University Press, Nanjing, 1–202 (in Chinese).
Ma, R. S., Shu, L. S. and Sun, J. Q. (1997) Tectonic evolution and mineralization of eastern Tianshan. Geological Publishing House, Beijing, 152–170 (in Chinese).
Mao, J. W., Yang, J. M., Han, C. M. and Wang, Z. L. (2002a) Metallogenic Systems of Polymetallic Copper and Gold Deposits and Related Metallogenic Geodynamic Model in eastern Tianshan, Xinjiang. Earth Sci.— J. China Univ. Geosci., 27, 413–424 (in Chinese with English abstract).
Mao, J. W., Yang, J. M., Qu, W. J., Du, A. D., Wang, Z. L. and Han, C. M. (2002b) Re–Os dating of Cu-Ni sulfide ores from Huangshandong deposits in Xinjiang and its geological significance. Miner. Depos., 21, 323–330 (in Chinese with English abstract).
Mao, J. W., Goldfarb, R. J., Wang, Y. T., Hart, C. J., Wang, Z. L. and Yang, J. M. (2005) Late Paleozoic base and precious metal deposits, East Tianshan, Xinjiang, China: characteristics and geodynamic setting. Episodes-Newsmagazine Int. Union Geol. Sci., 28, 23–30.
Marschik, R. and Fontboté, L. (2001) The Candelaria-Punta del Cobre iron oxide Cu-Au (-Zn-Ag) deposits, Chile. Econ. Geol., 96, 1799–1826.
Mathur, R., Ruiz, J. and Tornos, F. (1999) Age and sources of the ore at Tharsis and Rio Tinto, Iberian Pyrite Belt, from Re–Os isotopes. Miner. Deposita, 34, 790–793.
Morelli, R. M., Creaser, R. A., Selby, D., Kelley, K. D., Leach, D. L. and King, A. R. (2004) Re–Os sulfide geochronology of the red dog sediment-hosted Zn-Pb-Ag deposit, Brooks Range, Alaska. Econ. Geol., 99, 1569–1576.
Morgan, J. W., Stein, H. J., Hannah, J. L., Markey, R. J. and Wiszniewska, J. (2000) Re–Os study of Fe-Ti-V oxide and Fe-Cu-Ni sulfide deposits, Suwa ki Anorthosite Massif, northeast Poland. Miner. Deposita, 35, 391–401.
Nozaki, T., Kato, Y. and Suzuki, K. (2010) Re–Os geochronology of the Iimori Besshi-type massive sulfide deposit in the Sanbagawa metamorphic belt, Japan. Geochim. Cosmochim. Acta, 74, 4322–4331.
Ohmoto, H. (1972) Systematics of sulfur and carbon isotopes in hydrothermal ore deposits. Econ. Geol., 67, 551–578.
Pirajno, F. (2009) Hydrothermal processes and mineral systems. Springer, London, 307p.
Pirajno, F., Mao, J. W., Zhang, Z. C., Zhang, Z. H. and Chai, F. M. (2008) The association of mafic-ultramafic intrusions and A-type magmatism in the Tian Shan and Altay orogens, NW China: implications for geodynamic evolution and potential for the discovery of new ore deposits. J. Asian Earth Sci., 32, 165–183.
Qi, L., Zhou, M. F., Wang, C. Y. and Sun, M. (2007) Evaluation of a technique for determining Re and PGEs in geological samples by ICP-MS coupled with a modified Carius tube digestion. Geochem. J., 41, 407–414.
Qi, L., Zhou, M. F., Gao, J. F. and Zhao, Z. (2010) An improved Carius tube technique for determination of low concentrations of Re and Os in pyrites. J. Anal. At. Spectrom., 25, 585–589.
Qi, S. J., Wang, D. L. and Liu, T. (2008) Division of metalloigenetic region-zones and minerogenic features of major dominant mineral products in Xinjiang. Xinjiang Geol., 26, 348–355 (in Chinese with English abstract).
Qin, K. Z., Fang, T. H., Wang, S. L., Zhu, B. Q., Feng, Y. M., Yu, H. F. and Xiu, Q. Y. (2002) Plate tectonics division, evolution and metallogenic settings in eastern Tianshan Mountains, NW China. Xinjiang Geol., 20, 302–308 (in Chinese with English abstract).
Qin, K. Z., Peng, X. M., San, J. Z., Xu, X. W., Fang, T. H., Wang, S. L. Yu, H. F. (2003a) Types of major ore deposits, division of metallogenic belts in eastern Tianshan, and discrimination of

potential prospects of Cu, Au, Ni mineralization. Xinjiang Geol., 21, 143–150 (in Chinese with English abstract).

Qin, K. Z., Zhang, L. C., Xiao, W. J., Xu, X. W., Yan, Z. and Mao, J. W. (2003b) Overview of major Au, Cu, Ni and Fe deposits and metallogenic evolution of the eastern Tianshan Mountains, Northwestern China. *In* Mao, J. W., Goldfarb, R. J., Seltmann, R., Wang, D. H., Xiao, W. J. and Hart, C. J. (eds.) Tectonic evolution and metallogeny of the Chinese Altay and Tianshan. IAGOD Guidebook Series 10, CERCAMS/NHM, London, 227–248.

Rui, Z. Y., Wang, L. S., Wang, Y. T. and Liu, Y. L. (2002) Discussion on metallogenic epoch of Tuwu and Yandong porphyry copper deposits in Eastern Tianshan Mountains, Xinjiang. Miner. Depos., 21, 16–22 (in Chinese with English abstract).

San, J. Z., Qin, K. Z., Tang, D. M., Su, B. X., Sun, H., Xiao, Q. H. and Liu, P. P. and Cao, M. J. (2010) Precise zircon U-Pb ages of Tulargen large Cu-Ni-ore bearing mafic-ultramafic complex and their geological implications. Acta Petrol. Sin., 26, 3027–3035 (in Chinese with English Abstract).

Schoenberg, R., Ngler, T. F. and Kramers, J. D. (2000) Precise Os isotope ratio and Re–Os isotope dilution measurements down to the picogram level using multicollector inductively coupled plasma mass spectrometry. Int. J. Mass Spectrom., 197, 85–94.

Selby, D., Kelley, K. D., Hitzman, M. W. and Zieg, J. (2009) Re–Os sulfide (bornite, chalcopyrite, and pyrite) systematics of the carbonate-hosted copper deposits at Ruby Creek, southern Brooks range, Alaska. Econ. Geol., 104, 437–444.

Shu, L. S., Charvet, J., Lu, H. F. and Laurent-Charvet, S. (2002) Paleozoic accretion-collision events and kinematics of deformation in the eastern part of the Southern-Central Tianshan belt, China. Acta Geol. Sin., 76, 308–323.

Smoliar, M. I., Walker, R. J. and Morgan, J. W. (1996) Re–Os ages of group IIA, IIIA, IVA, and IVB iron meteorites. Science, 271, 1099–1102.

Song, Z. J. (1985) The formative conditions and mineralization of a group of magnetite deposits in volcanic -intrusive complex region near Hami, Xinjiang. Bull. Xi'an Inst. Geol. Min. Res., Chin. Acad. Geol. Sci., 9, 58–73 (in Chinese with English abstract).

Song, Z. J., Ren, B. C., Wang, X. Q., Wei, S. E., Yang, S. L. and Yao, A. M. (1983) The metallogenesis of Yamansu, Heifengshan, Shaquanzi Fe deposits in the volcanic-intrusive complex area of the southern margin of the eastern section of north Tianshan, Xinjiang. Annu. Chin. Acad. Geol. Sci., Suppl., 114–115 (in Chinese).

Stein, H. J., Sundblad, K., Markey, R. J., Morgan, J. W. and Motuza, G. (1998) Re–Os ages for Archean molybdenite and pyrite, Kuittila-Kivisuo, Finland and Proterozoic molybdenite, Kabeliai, Lithuania: testing the chronometer in a metamorphic and metasomatic setting. Miner. Deposita, 33, 329–345.

Stein, H. J., Morgan, J. W. and Schersten, A. (2000) Re–Os dating of low-level highly radiogenic (LLHR) sulfides: the harnas gold deposit, Southwest Sweden, records continental-scale tectonic events. Econ. Geol., 95, 1657–1671.

Suzuki, K., Shimizu, H. and Masuda, A. (1996) Re–Os dating of molybdenites from ore deposits in Japan: implication for the closure temperature of the Re–Os system for molybdenite and the cooling history of molybdenum ore deposits. Geochim. Cosmochim. Acta, 60, 3151–3159.

Walker, R. J., Morgan, J. W., Horan, M. F., Czamanske, G. K., Krogstad, E. J., Fedorenko, V. A. and Kunilov, V. E. (1994) Re–Os isotopic evidence for an enriched-mantle source for the Noril'sk-type, ore-bearing intrusions, Siberia. Geochim. Cosmochim. Acta, 58, 4179–4197.

Wang, D. H., Li, C. J., Chen, Z. H., Chen, S. P., Xiao, K. Y., Li, H. Q. and Liang, T. (2006a) Metallogenic characteristics and direction in mineral research in east Tianshan, Xinjiang, China. Geol. Bull. China, 25, 910–915 (in Chinese with English abstract).

Wang, J. B., Wang, Y. W. and He, Z. J. (2006b) Ore deposits as a guide to the tectonic evolution in the East Tianshan Mountains, NW China. Geol. China, 33, 461–469 (in Chinese with English abstract).

Wang, L. S., Li, H. Q., Liu, D. Q. and Chen, Y. C. (2005) Geological characteristics and mineralization epoch of Weiquan silver (copper) deposit, Hami, Xinjiang, China. Miner. Depos., 24, 280–284 (in Chinese with English abstract).

Windley, B. F., Allen, M. B., Zhang, C., Zhao, Z. Y. and Wang, G. R. (1990) Paleozoic accretion and Cenozoic redeformation of the Chinese Tien Shan range, central Asia. Geology, 18, 128–131.

Wu, H., Li, H. Q., Mo, X. H., Chen, F. W., Lu, Y. F., Mei, Y. P. and Deng, G. (2005) Age of the Baishiqun mafic-ultramafic complex, Hami, Xinjiang and its geological significance. Acta Geol. Sin., 79, 498–502 (in Chinese with English abstract).

Xia, L. Q., Xia, Z. C., Xu, X. Y., Li, X. M., Ma, Z. P. and Wang, L. S. (2002a) Some thoughts on the characteristic of Paleozoic ocean-continent transition from Tianshan mountains. Northwest. Geol., 35, 9–20 (in Chinese with English abstract).

Xia, L. Q., Zhang, G. W., Xia, Z. C., Xu, X. Y., Dong, Y. P. and Li, X. M. (2002b) Constraints on the timing of opening and closing of theTianshan Paleozoic oceanic basin: evidence from Sinian and Carboniferous volcanic rocks. Geol. Bull. China, 21, 55–62 (in Chinese with English abstract).

Xia, L. Q., Xu, X. Y., Xia, Z. C., Li, X. M., Ma, Z. P. and Wang, L. S. (2003) Carboniferous post-collisional rift volcanism of the Tianshan Mountains, northwestern China. Acta Geol. Sin., 77, 338–360 (in Chinese with English abstract).

Xia, L. Q., Xu, X. Y., Xia, Z. C., Li, X. M., Ma, Z. P. and Wang, L. S. (2004) Petrogenesis of Carboniferous rift-related volcanic rocks in the Tianshan, northwestern China. Geol. Soc. Am. Bull., 116, 419–433.

Xia, L. Q., Xia, Z. C., Xu, X. Y., Li, X. M. and Ma, Z. P. (2008a) Relative contributions of crust and mantle to the generation of the Tianshan Carboniferous rift-related basic lavas, northwestern China. J. Asian Earth Sci., 31, 357–378.

Xia, L. Q., Xu, X. Y., Xia, Z. C., Li, X. M. and Ma, Z. P. (2008b) Petrogenesis of Carboniferous-early Permian rift-related volcanic rocks in the Tianshan and neighboring areas, northwestern China. Northwest. Geol., 41, 1–68 (in Chinese with English abstract).

Xiao, W. J., Zhang, L. C., Qin, K. Z., Sun, S. and Li, J. L. (2004) Paleozoic accretionary and collisional tectonics of the Eastern Tianshan (China): implications for the continental growth of central Asia. Am. J. Sci., 304, 370–395.

Xiao, W. J., Windley, B. F., Huang, B. C., Han, C. M., Yuan, C., Chen, H. L., Sun, M., Sun, S. and Li, J. L. (2009) End-Permian to mid-Triassic termination of the accretionary processes of the southern Altaids: implications for the geodynamic

evolution, Phanerozoic continental growth, and metallogeny of Central Asia. Int. J. Earth Sci., 98, 1189–1217.

Xiao, X. C., Tang, Y. Q., Feng, Y. M., Zhu, B. Q., Li, J. Y. and Zhao, M. (1992) Tectonic evolution of the Northern Xinjiang and its adjacent regions. Geological Publishing House, Beijing, 169p (in Chinese).

Xiao, Y. (2003) The geological characteristics and ore-finding oritention of Shaquanzi Cu deposit, Hami, Xinjiang. Xinjiang Nonferrous Metals, 26, 9–11 (in Chinese with English abstract).

Xie, J. C., Yang, X. Y., Du, J. G., Du, X. W., Xiao, Y. L., Qu, W. J. and Sun, W. D. (2009) Re–Os precise dating of pyrite from the Xinqiao Cu-Au-Fe-S deposit in Tongling, Anhui and its implications for mineralization. Chin. J. Geol., 44, 183–192 (in Chinese with English abstract).

Xu, X. T., Yuan, W. M., Gong, Q. J., Wu, F. F., Huang, Z. X. and Deng, J. (2010) The analysis of zircon Ffission track's ore-forming epoch in Shaquanzi copper-iron deposit, Xinjiang. China. Min. Mag., 19, 105–108 (in Chinese with English abstract).

Xu, X. W., Ma, T. L., Sun, L. Q. and Cai, X. P. (2003) Characteristics and dynamic origin of the large-scale Jiaoluotage ductile compressional zone in the eastern Tianshan Mountains, China. J. Struct. Geol., 25, 1901–1915.

Yan, W. Y. (1985)) The characteristics of early Carboniferous volcanic island arc and mineralization in the east setion of Tianshan. Xinjiang Geol., 3, 49–51 (in Chinese with English abstract).

Yang, X. K., Tao, H. X., Luo, G. C. and Ji, J. S. (1996) Basic features of plate tectonics in east Tianshan of China. Xinjiang Geol., 14, 221–227 (in Chinese with English abstract).

Yang, X. K., Ji, J. S., Luo, G. C. and Tao, H. X. (1997) Plate tectonics and forming law of the metallic ore deposits in eastern Tianshan. J. Xi'an Coll. Geol., 19, 34–42 (in Chinese with English abstract).

Yang, X. K., Cheng, H. B., Ji, J. S., Cheng, Q. and Luo, G. C. (1999) Analysis on gold and copper ore-forming system with collision orogeny of eastern Tianshan. Geotectonica Et Metallogenia, 23, 315–332 (in Chinese with English abstract).

Yang, Z. F., Luo, Z. H., Lu, X. X., Cheng, L. L. and Huang, F. (2011) Discussion on significance of Re content of molybdenite in tracing source of metallogenic materials. Miner. Depos., 30, 654–674 (in Chinese with English abstract).

Zeng, C. L. (1962) Preliminary exploration report of the Shaquanzi Fe-Cu deposit. Hami, Xinjiang (in Chinese).

Zhang, L. C., Xiao, W. J., Qin, K. Z., Ji, J. and Yang, X. (2004) Types, geological features and geodynamic significances of gold-copper deposits in the Kanggurtag metallogenic belt, eastern Tianshan, NW China. Int. J. Earth Sci., 93, 224–240.

Zhang, L. C., Xiao, W. J., Qin, K. Z., Qu, W. J. and Du, A. D. (2005) Re–Os isotopic dating of molybdenite and pyrite in the Baishan Mo-Re deposit, eastern Tianshan, NW China, and its geological significance. Miner. Deposita, 39, 960–969.

Zhang, L. C., Xiao, W. J., Qin, K. Z. and Zhang, Q. (2006) The adakite connection of the Tuwu-Yandong copper porphyry belt, eastern Tianshan, NW China: trace element and Sr-Nd-Pb isotope geochemistry. Miner. Deposita, 41, 188–200.

Zhang, L. C., Qin, K. Z. and Xiao, W. J. (2008) Multiple mineralization events in the eastern Tianshan district, NW China: isotopic geochronology and geological significance. J. Asian Earth Sci., 32, 236–246.

Zhang, Z., Zhou, G., Kusky, T. M., Yan, S., Chen, B. and Zhao, L. (2009) Late Paleozoic volcanic record of the Eastern Junggar terrane, Xinjiang, Northwestern China: major and trace element characteristics, Sr-Nd isotopic systematics and implications for tectonic evolution. Gondwana Res., 16, 201–215.

Zhang, Z. M., Liou, J. G. and Coleman, R. G. (1984) An outline of the plate tectonics of China. Bull. Geol. Soc. Am., 95, 295–312.

Zhou, J. Y., Cui, B. F., Xiao, H. L., Chen, S. Z. and Zhu, D. M. (2001) Kangguertag-Huangshan Collision Zone of Bilateral Subduction and Its Metallogenic Model and Prognosis in Xinjiang, China. Volcanol. Miner. Resour., 22, 252–263 (in Chinese with English Abstract).

Zhou, M. F., Michael Lesher, C., Yang, Z., Li, J. and Sun, M. (2004) Geochemistry and petrogenesis of 270 Ma Ni-Cu-(PGE) sulfide-bearing mafic intrusions in the Huangshan district, Eastern Xinjiang, Northwest China: implications for the tectonic evolution of the Central Asian orogenic belt. Chem. Geol., 209, 233–257.

Zhou, M. F., Zhao, J. H., Jiang, C. Y., Gao, J. F., Wang, W. and Yang, S. H. (2009) OIB-like, heterogeneous mantle sources of Permian basaltic magmatism in the western Tarim Basin, NW China: implications for a possible Permian large igneous province. Lithos, 113, 583–594.

Zhou, T. F., Yuan, F., Zhang, D. Y., Fan, Y., Liu, S., Peng, M. X. and Zhang, J. D. (2010) Geochronology, tectonic settings and mineraltion of granitoids in Jueluotage area, eastern Tianshan, Xinjiang. Acta Petrol. Sin., 26, 478–502 (in Chinese with English abstract).